Experimental and Numerical Study of Localized Pitting Effect on Compressive Behavior of Tubular Members

Renhua Wang[1.]*, Haichao Guo[1.], R Ajit Shenoi[2.]

wrhchina@163.com

1. Department of Civil Engineering, Jiangsu University of Science of Technology, Zhenjiang 212003, China
2. Southampton Marine and Maritime Institute, University of Southampton, Boldrewood Innovation Campus, Southampton SO16 7QF, UK

Abstract

Locally pitted tubular members are usually considered as stub columns to assess the ultimate strength. However, it is not suitable for those with relatively larger slenderness ratios as their failure behavior is more complex and closely related to corrosion features of localized pitting. This paper presents compressive column tests on locally pitted tubular members of a moderate slenderness ratio. Corrosion pits were artificially introduced on local surface of the members, forming corrosion patches with various corrosion features. A numerical modelling method was proposed to reproduce the test specimens. Localized pitting damage was proven to cause substantial declines in the load deformation capacity and ultimate strength, and have a significant effect on the failure mode. The failure of a pitted member is mostly initiated by local buckling after yielding in the corrosion patch, concurrent with pitting closure, and even shear cracking of member wall due to the perforated pits. Moreover, shape change of the corrosion patch most likely results in the failure mode to alter from column buckling to local buckling or interactive buckling. The shape ratio of the corrosion patch is one of the critical factor to influence the ultimate strength of locally pitted members. The proposed modelling method is applicable for extensive stochastic simulations so as to develop an empirical formula and to clarify the probabilistic characteristics of ultimate strength.

Keywords: tubular member; localized pitting damage; compressive column test; random pitting modelling; ultimate strength; failure mode

1. Introduction

Corrosion is an electrochemical process promoting corrosion pits arise on metal surface of steel members. This is one of the common damages for tubular members of offshore structures in the splash zone due to the shortage of corrosion control measure to resist the complex and variable corrosive environment [1]. Pitting corrosion normally appears on a member in two forms such as widely scattered pitting that occurs over the entire surface of the member (widespread pitting), and localized region of pitting (localized pitting) [2]. Over time, corrosion damage within pits can result in localized indentation or even perforation of member wall, and thus makes local stress field nearby the pits intensified, likely causing fracture and break in the member [3, 4]. Many failure accidents of tubular member structures have been reported resulting from corrosion damage synergetic with axial stress [5, 6]. Moreover, the safety of such structural system is influenced by the uncertainties of geometric and mechanical properties in members and joints [7, 8] Therefore, the damage of local or overall corrosion should be taken into account in determining the residual strength of corroded tubular members.

It is vital to model the irregular morphology of corrosion damage for ultimate strength assessment. However, the cost of corrosion inspection makes it unrealistic to obtain detailed mapping of actual corrosion, although many nondestructive measurement methods such as gamma rays and ultrasonic testing exist [9]. There is no adequate information to determine strength of corroded tubular members for inclusion of requirements in the International Standard [10]. As a common solution, the irregular corrosion is simplified into uniform corrosion for the ultimate strength assessment of damaged members [2, 11]. A damaged member is assigned with an equivalent thickness (uniform corrosion) that is uniformly reduced over the whole member [10]. And the member with reduced thickness can be treated as an undamaged one to evaluate ultimate strength, leading to a conservative prediction. Base on such method, numerous experimental and numerical studies have been conducted to explore the ultimate strength of corroded members with localized uniform corrosion, such as compressive strength of short tubular members [12], H-shaped short columns [13, 14], unstiffened plates [15] and stiffened panels [16], and the flexural capacity or failure pressure of pipeline structures [17, 18]. Notably, the irregularity of localized pitting has not been properly dealt with in the existing studies but replaced by localized uniform corrosion. Even so,

the simplified corrosion caused a significant reduction of ultimate strength being closely related to the shape of locally corroded area (corrosion patch), member size and loading pattern.

Corrosion may perforate the wall of a member, leading to an eccentricity in the centroid of its cross section and then extra secondary bending moment [9]. Changing the location of a perforation along the length of a member was considered influential to the reduction of ultimate strength [19]. As for in-service offshore structures, corrosion more often induces uneven metal loss on the surface of a member rather than perforations, as shown in Figure 1. Otherwise, the damaged member needs to be replaced by a new one prior to occurrence of such serious damage. In respect to pitting effect, extensive experiments have been carried out to study material properties of tensile coupons [20, 21], ultimate bending capacity of hold frames [22, 23] and ultimate strength of stiffened panels [24, 25]. These studies mostly focused on widespread pitting that was mimicked by artificial pits drilled by a hand drill that were regularly distributed over the tested specimens. It was suggested that the reduction of ultimate strength was mainly dependent on volume loss of material due to the pitting corrosion instead of random nature of pitting corrosion. In order to simulate pitting damage more really, localized pitting in a random distribution was drilled on stub columns of tubular section [26]. It was found that local buckling more easily arose in the locally pitted area under axial compression, and the reduction of ultimate strength of the locally pitted stub column was decided by area loss of the weakest section. However, some studies claimed that the adverse effect of localized pitting damage is closely related to the corrosion depth as well as the width and length of corroded area [27]. Recently, a stochastic modelling method has been proposed to simulate the random nature of widespread pitting [28]. Such method has been calibrated against column tests on pitted tubular members of medium slenderness ratios of which widespread pitting was simulated by corrosion pits regularly drilled and widely scattered over the entire surface of members. It was confirmed that the widespread pitting damage causes a striking strength reduction up to 20.7% more than that caused by uniform corrosion under the same volume loss of corroded material [29]. In addition, the widespread pitting can result in a great variation of ultimate strength due to the effect of random nature of pitting damage, but probabilistic characteristics of the variant ultimate strength can be obtained by performing stochastic simulation [30]. Being different from widespread pitting that mainly causes material loss in a member, localized pitting in the form of patch corrosion has great

uncertainties in the size, distribution location and shape of the locally corroded area besides the material loss. These influential factors have not been properly considered in the existing studies, but they may take major responsibility to the inconsistency of reported results. However, there are very few studies relevant to these issues, especially for tubular members of moderate slenderness ratios, despite some insights into corrosion effect on structural members. In particular, no experimental studies have been carried out in open literatures to systematically investigate the combined effects from the shape of corrosion patch and the volume loss of corroded material.

The paper presents a test programme on locally pitted tubular members of medium length under axial compression. These members were mechanically introduced with/without localized pitting damage in the form of corrosion patch with various corrosion features. A novel modelling method was proposed to replicate the test specimens by modelling detailed irregularity of pitting corrosion. Numerical models built by the modelling method were verified upon the benchmark tests of locally pitted members. This was followed by further numerical studies to clarify the effects of the depth, size, location and shape of the corrosion patch on compressive behavior and ultimate strength. Finally, analytical methods in open literatures and the proposed modelling method in this paper were further calibrated against the experimental results.

2. Experimental study

All the tested specimens were cut from the same seamless steel tube with a nominal outer diameter (D) of 60 mm and wall thickness (t) of 4.3 mm. The ratio of tube diameter to wall thickness (D/t) was about 14 belonging to Class 1 cross-section according to the slenderness limits in EN1993-1-1 [31]. Localized pitting to the specimens was simulated by introducing 40 or 120 corrosion pits that were randomly and artificially drilled on local external surface of each pitted member through a hand drill. The degree of pitting intensity (DOP) in all the pitted members was determined to be identical to ensure that the effect of one corrosion feature can be studied under the same condition. A total of twelve specimens were tested including three intact specimens (without pits) and nine pitted specimens. The matrix of test specimens is shown in Table 1. The test setup and procedures, and obtained key results such as ultimate loads, load deformation histories and failure modes are fully reported in this section.

2.1 Test specimens

A typical intact specimen and pitted one are illustrated in Figure 2. The parameters needed to describe one corrosion patch include the length (l), width (θ) and location (h) of the corrosion patch; and member length (L) and outside diameter (D). Corrosion pits were randomly drilled on the local surface of a specimen. The edges of the corrosion patch surrounding all the corrosion pits forms a rectangle if the outside surface of the member was unfolded, as shown in Figure 3. Hence, the shape ratio, SR, defined by the ratio of the length to width of the corrosion patch as Eq. (1) can be used to reflect the shape of the corrosion patch.

$$SR = \frac{\mu_L L}{\mu_P \pi D} = S_r\left(\frac{L}{\pi D}\right) \tag{1}$$

where μ_L is the ratio of the length of the corrosion patch to the member length, equal to l/L, while μ_P is the ratio of the width of the patch to the member perimeter (πD), equal to $\theta/360$. Therefore, the relative shape ratio (S_r) derived from normalized shape ratio (μ_L/μ_P) is representative of the shape of the corrosion patch. The virgin area of the corrosion patch is:

$$A = \mu_L L \times \mu_P \pi D = \mu_L \mu_P (\pi D L) \tag{2}$$

Commonly, the DOP and the degree of corroded volume loss (DOV) defined on the whole surface of a member are used to describe the damage level of widespread pitting where corrosion pits are widely distributed over the entire surface of the member [29]. As for localized pitting, it seems more rational to define the level of pitting damage according to the size of the corroded area. Therefore, the DOP is determined in terms of the area of the corrosion patch as follows:

$$DOP = \frac{A_c}{A} \times 100(\%) = \frac{1}{\mu_L \mu_P D L} \sum_{i=1}^{K} r_i^2 \times 100(\%) \tag{3}$$

Correspondingly, the DOV within the corrosion patch can be defined as:

$$DOV = \frac{V_c}{V} \times 100(\%) = \frac{1}{2\mu_L \mu_P R L t} \sum_{i=1}^{K} d_i r_i^2 \times 100(\%) \tag{4}$$

where A_c and V_c denote the losses of locally corroded area and volume due to corrosion pits within the corrosion patch, respectively, while A and V are the original area and volume corresponding to the corrosion patch; t is the virgin wall thickness of the member, and R is the radius of intermediate

surface of the member, equal to (D-t)/2. K is the number of the corrosion pits in the corrosion patch, and r_i and d_i are the radius and depth of i^{th} pit, respectively.

The nomenclature used to identify each specimen in the test program consisted of the length (l) and width (θ) of the corrosion patch, and a reserved label to index the specified specimen in a group of akin specimens with relevant attributes, as shown in first column of Table 1. Hence, Specimens 0-0-1, 0-0-2 and 0-0-3 are a group of non-pitted (intact) specimens that were control specimens to define the extent of strength reduction for pitted members. Correspondingly, Specimens 1/4-120-1, 1/4-120-1 and 1/4-120-3 form a set of pitted specimens with the same pitting damage. In such group, "1/4" and "120" indicate that the corrosion patch had a length of L/4 and a width of 120°. Here the same column tests were performed on three identical specimens respectively for the intact or pitted specimens. It aimed to check the repeatability and variation of the experimental studies. However, Specimens 1/4-360-M, 1/4-360-B and 1/4-360-E were used to study the effect of the location of the corrosion patch that was varied along the length of a specimen. Meanwhile, the corrosion patch had a length of L/4 and width of 360°, and was situated at mid-height, both ends or one end. Specimens 1-90, 3/4-120 and 1/4-360-M had the same corroded area but with different patch shapes. Specimen 1/4-120-T had the same corrosion patch as Specimens 1/4-120 series but with perforated pits to simulate severe corrosion damage. Notably, all the pitted members were introduced with the same degree of pitting intensity, DOP 15% that is the critical value to decide whether or not to perform a corrosion inspection on in-service marine and offshore structures [32]. The corrosion pits were mechanically drilled using a drill bit of a diameter of 6 mm. More specified attributes used to group the test specimens with relevant corrosion features are shown in Table 2. The details on pitting patterns in all the test specimens can be found in Figure 3, illustrated in a way easy to reproduce and validate in the numerical modelling for further studies.

Each specimen was fabricated with the same length (L) of 480 mm whose actually measured size are listed in Table 1. The mean values of the diameter and thickness of members were 59.82 and 4.33 mm, respectively, while the mean depth and diameter of corrosion pits were 2.12 and 6 mm, respectively. The effective length of the test specimen was half of total column length with reference to both hinged ends because both ends of each test specimen was mounted on the testing

machine via a set of devised stiff connecters as fixed ends. The slenderness ratios of all the test specimens were the same value equal to about 12.2.

Material properties of the test specimens were determined via prior tensile coupon testing before conducting the compressive column tests. Four material coupons were tested under uniaxial tension. The average stress-strain curves of the tensile coupons are shown in Figure 4(a). One of them with the lowest yield stress was used to represent the material constitutive model, as shown in Figure 4(b), together with the corresponding true stress-strain curve. And the latter was utilized for the subsequent nonlinear analyses. Yield stress (σ_y) of the steel material of members took the stress corresponding to 0.2% plastic strain because the average stress-strain curves of all tensile coupons had no obvious yield plateau. The $\sigma_{0.2}$ was 318 MPa, while ultimate stress (σ_u) was 485 MPa; the Young's modulus (E) was 118 GPa.

2.2 Compressive column tests

Compressive column tests were carried out in the Engineering Mechanics Laboratory at the Jiangsu University of Science and Technology. A photograph of the test setup used in this study before and after seating a test specimen is shown in Figure 5. Each specimen was positioned in testing machine, with a 10 mm thick steel endplate at each end that were weld to the specimen during specimen preparation. The endplate at each end was bolted to a cap-shaped connecter that was used to fasten the test specimen with testing machine. The connecter was made up of two 10 mm thick steel square plates that were bolted together, and one of which had an incision hole fit to the size of cylindrical platen on the support pedestal, as shown in Figure 5. The specimen was shimmed as necessary to correct any misalignments and be vertically mounted onto the testing machine.

Compressive column tests were conducted using a servo electro-hydraulic universal machine (YNS-1000) with loading capacity of 1000 kN. Axial load was applied through a load cell exerting a uniformly distributed load to the topside cap-shaped connecter. The axial load and displacement were automatically measured through inbuilt force and displacement sensors in the testing system.

The same loading procedures were adopted for all the test members. A small alignment load of 10 kN was applied before starting a compressive column test to ensure the fully contact between the cylindrical platens and the cap-shaped connecters. After completely unloading the alignment load,

the loading on the specimen then commenced under displacement control at a constant rate of 3 mm/min. The test continued beyond the ultimate state but with axial shortening no more than 30 mm at the post-ultimate load stage.

For an intact specimen, a total of 12 electrical resistance gauges of 3-mm gauge length were used to measure the longitudinal strain, as shown in Figure 6, forming three levels of rings at the top, mid-height and bottom of the specimen. For each level, four gauges were placed around the circumference of the cross section. As for a pitted specimen, strain distribution in the corrosion patch was more complex due to stress irregularity caused by random corrosion pits. Hence, more strain gauges were used at the mid-height, namely, six gauges for the partially pitted specimen and eight gauges for the fully pitted specimen. On the basis of the previous study [29], such measure scheme of strain gauges was thought enough to capture the change of strain distribution along the length of the specimen.

2.3. Experimental results

2.3.1. Load deformation behavior

Figure 7 shows the load deformation behavior of the control specimens (Specimens 0-0 series) and typical pitted specimens (Specimens 1/4-120 series). There is no distinct difference in the load deformation behavior of the intact and pitted specimens at the elastic behavior stage. However, the load carrying capacity and the ductility of the pitted specimens began to steeply decline, especially at the post-collapse stage. The mean ultimate loads of the intact and pitted specimens were 318 and 299 kN, while the limit axial deformations were 16.5 and 12.7 mm, respectively. The percentage reduction of mean ultimate load and deformability of the pitted specimen were about 5.97% and 23.7%, compared with the control specimen. Recalling the experiments on tubular members with widespread pitting reported in [29], Specimens IC3010d3.3 and UC3010d3.4 were subject to pitting damage of DOP 12.46 % that was less than DOP 15% in the pitted specimens studied herein. For the two specimens, the widespread pitting leaded to larger reductions of ultimate loads of 16.9% and 13.3%, but smaller reductions of deformations of 3.3% and -1.8%, respectively. It can thus be concluded that random pitting damage can cause significant decrease in the ultimate load and axial deformability of tubular members. However, in comparison to the widespread pitting, the localized pitting caused a larger reduction in the axial deformability but a smaller reduction in the ultimate

load. The difference in the load deformation behavior can be attributed to the failure mode affected by the different forms of pitting damage. Actually, the local buckle that always initiated in locally pitted area in the test specimens with localized pitting had a significant impact to their compressive behavior.

Figure 8 further shows load deformation behavior of the test specimens that were grouped in terms of the attributes listed in Table 2 for various corrosion features. It is evident that corrosion features such as the depth, size, location and shape of the corrosion patch had a significant effect on the load deformation behavior. Localize pitting damage resulted in a prominent degradation of compressive behavior. The adverse effect was pronounced after yielding in the locally pitted area occurred, and became extremely serious at the post-collapse stage. On the whole, the localized pitting caused significant declines in the yield load, ultimate load and deformability, and structural stiffness, as observed in the experiments of corroded plated structures [33].

2.3.2. Failure mode

Intact specimens (0-0 serials) failed by global buckling in the mode of long column failure, as shown in Figure 9(a). Local buckles formed simultaneously at the top and lower ends of the intact specimen close to its endplates, which resembled an elephant-foot surrounding full circumference. Thereafter, wall wrinkle occurred on the compressive side at a slight shift away from the mid-height after compressive ultimate load reached. In general, the failure modes of intact specimens were mainly dominated by global column buckling.

For all pitted specimens, except Specimen 1-90, the failure modes were interactive buckling due to the interaction of local buckling and column buckling. Figure 9(b) shows the typical failure mode of a pitted specimen (1/4-120-3). The local buckling and column buckling were observed to occur almost at the same time. The local buckling caused an inward movement of member wall in the corrosion patch. It is worthy of note that the inward mode of buckling did not initiate on the cross-section denoted by four red points for Specimen 1/4-120-3 shown in Figure 3, despite this cross-section was weakest cross section of the specimen. Instead, the onset of yielding and local buckling arose on an irregular section jointing multiple adjacent corrosion pits at the top of the corrosion patch, due to stress interaction between these corrosion pits. As the axial deformation was continued, these pits were observed to squish and even completely close up. The consequence of the

yielding and local buckling was a loss of capacity. It follows that the weakest cross-section would not necessarily lead to the failure and decide the ultimate load of locally pitted members of medium length. This is quite different from the case reported on corroded stub columns that collapsed only by local buckling [26].

For Specimen 1-90, the localized pitting where corrosion pits were randomly scattered along the entire length but in the partial hoop had no influence on the failure mode, as shown in Figure 9(c). The specimen collapsed by column buckling like an undamaged member, although localized pitting existed in the partial surface denoted by gauges M_5, M_1 and M_6. In such case, the initial deflection rather than pitting damage dominated the failure mode of the specimen, as observed in the tests of corroded plated structures [34]. In fact, the column buckling is the main failure mode for the tubular members with widespread pitting where corrosion pits were widely distributed over the member in a uniform or stagger pitting pattern [29]. Therefore, the distribution pattern of pitting damage has a critical impact to the failure mode. In contrast to the widespread pitting, the localized pitting shows more complex effect on the compressive behavior, for it may cause the change of failure mode due to the change of a certain corrosion feature.

In addition, the failure mode of a pitted specimen was significantly influenced by the depth of corrosion pits, as shown in Figure 10. For Specimen 1/4-120-3 with non-perforated pits, multiple pits were squashed to cause pitting closure, eventually leading to yielding and then local buckling to propagate around the circumference. However, in the case of severe corrosion, for Specimen 1/4-120-T with perforated pits, shear cracking was observed to occur in the region between several adjacent pits due to serious stress interaction between the perforated pits, leading to the failure of the specimen.

2.3.3. Load strain behavior

All test specimens, except Specimen 1/4-120-T, exhibited high deformation capacities. Axial strains were obtained at top, mid-height and bottom of test specimens using measure scheme shown in Figure 6. Figure 11 and Figure 12 plot typical load strain behavior of intact and pitted specimens, respectively.

In the intact specimens, initial deflection universally existed, for tensile strains were observed to momentarily occur at mid-height even at elastic behavior stage as shown in the middle row of

Figure 11. And the larger tensile strain meant the larger initial deflection. As the axial deformation was continued, persistent compressive strains appeared in lieu of the ephemeral tensile strains. And yielding was observed to occur due to P-Delta effect with an obvious lateral deformation at the mid-height. Development of the lateral deformation made the compressive strains turn to be tensile with a sudden strain reversal at the collapse stage, as shown in Figure 11. This meant the onset of column buckling, the corresponding load of which was 250 kN about 80% of the ultimate load.

For the pitted specimens, the load strain behavior displayed a more complex change, as they collapsed due to the interaction of local buckling and column buckling. As shown in Figure 12, a sudden reversal of the compressive strains first occurred at mid-height due to the column buckling that was accompanied by local buckling initiating in the corrosion patch. As the axial shortening was continued, the yielding and local buckling became more extensive and propagated near the locally corroded section. A new sudden reversal of compressive strains may emerge at one or both quarter heights that approximated to the points of reverse bending.

2.3.4. Ultimate load

Table 3 shows a summary of ultimate loads of all the test specimens. Figure 13 illustrates the effects of corrosion features including the depth, size, location and shape of the corrosion patch on the reduction of ultimate strength. It should be noted that Specimens 0-0 and 1/4-120 in Figure 13 were representative of their akin specimens corresponding to the control and pitted specimens. Hence, the mean values of their ultimate loads were determined according to the test results of three akin specimens. The degradation ratios of ultimate loads of pitted specimens were then decided in terms of the mean ultimate load of 0-0 (318 kN).

Figure 13(a) shows that pit depth of the corrosion patch had a significant effect on the reduction of ultimate strength of test specimens even if pitting intensity was relatively low (DOP 15%). Specimens 1/4-120 and 1/4-120-T had ultimate loads of 299 kN and 264 kN, respectively. The pit depth in Specimen 1/4-120 was about 50% of wall thickness, while it caused a degradation ratio about 6%. However, the perforated pits in Specimen 1/4-120-T had the degradation ratio sharply increased up to 17%.

Figure 13(b) shows that it seemed ambiguous for the size effect on the reduction of ultimate strength. Compared with specimen 1/4-120, the length increase of the corrosion patch in Specimen

3/4-120 caused a slightly larger strength reduction, but the width increase in Specimen 1/4-360-M did not cause a decrease but caused a slight increase in the ultimate load. The anomaly in the size effect should be attributed to the variation of test results caused by random nature of pitting distribution.

Figure 13(c) displays that the location change of the corrosion patch had some effects on the ultimate load. In particular, in Specimen 1/4-360-B shown in Figure 3, it can cause more serious reduction in ultimate strength if the single patch was separated into a dual-patch pattern. This was due to the fact that the dual-patch pattern can cause simultaneous degradations in the support stiffness from the endplates at both ends of the specimen.

Figure 13(d) indicates that the shape effect of the corrosion patch had a remarkable effect one the ultimate strength. However, the effect was fluctuant due to the random nature of pitting damage. It might partially be due to the manufacturing errors in member size and pit depths as well as initial deflection. Nevertheless, it can be inferred that the shape effect may be more pronounced for the pitting intensity higher than DOP 15% studied herein. As for the corrosion patch having the same pitting damage but with varying shape, the resulting strength reduction was dependent on the shape ratio (S_r) of the corrosion patch. The corrosion patch in Specimen 1-90 had a shape ratio, $S_r = 4$ that was the maximum shape ratio for its akin specimens, leading to the highest ultimate strength.

Overall, the effect of a certain corrosion feature except pit depth on the reduction of ultimate strength is not sufficiently clear due to the combined influence of manufacturing error and random nature of pitting damage. It is hard to quantitate the reduction of ultimate strength due to localized pitting damage if only based on the limited test results. Limitations in experimental studies make it necessary to conduct further numerical analyses to supplement data pool for the clarification on the complex effect of localized pitting damage.

3. Numerical study

Numerical studies were carried out using the modelling method adopted from the patent of Chinese State Patent Office [28]. The modelling method has been validated upon pitted members with widespread pitting damage [29, 30]. Given some modifications were done on such method, it can be used to model the localized pitting corrosion where corrosion pits were randomly scattered on local surface of tubular members. The numerical modelling was carried out using finite element

(FE) analysis package ANSYS. FE models were first validated against the corresponding test results reported in the above section, and then were used to conduct numerical studies to clarify the effects of the depth, size, location and shape of the corrosion patch on the reduction of ultimate strength.

3.1. Modelling method

Cylindrical surface of a tubular member is a rectangle (plate) if unfolded along any generatrix, as shown in Figure 14. Therefore, the generatrix *a*-*b* was split into two opposite edges *a*'-*b*' of the unfolded plate of a length of *L*. And the circumference at both ends of the member formed other two opposite edges of the ulfolded plate *a*'-*a*' and *b*'-*b*' of a width of πD equal to the perimeter.

The random nature in pitting distribution of a pitted member can be approximated by randomly assigning corrosion pits onto the pitted area of the unfolded plate. To achieve this goal, the unfolded surface was split with a series of grids of identical sizes. And each corner of the grids was a possible position to seat one corrosion pit. Figure 14 illustrates the one-to-one mapping between the corner of a grid *i*' on the unfolded plate and the corrosion pit *i* on the member. Usually, the unfolded plate can be partitioned with *M* grids along its length and *N* grids along its width by modular lengths. A matrix of position array [*U*] with *M*+1 rows and *N* columns was defined to record the locations of corners of all the grids. In the array [*U*], the locations of all random corrosion pits can be indexed through a position vector [30] as:

$$P = ((x_1, z_1), (x_2, z_2), \dots, (x_n, z_n))^T \quad (5)$$

where (x_i, z_i) are the coordinates of one corrosion pit on the unfolded plate, represented by a set of row and column numbers of the array [*U*].

With respect to random nature of pitting size, it included the width (diameter), *w*, and depth, *d*, of a corrosion pit, composing a size vector [30] as:

$$S = ((w_1, d_1), (w_2, d_2), \dots, (w_n, d_n))^T \quad (6)$$

The random location and size in Eqs. (5) and (6) were determined via a simple random number generator. The specified position of one single pit was attained by multiplying the column and row numbers from Eq. (5) and the corresponding moduli that was used to partition the unfolded plate. Suppose the modular lengths in width and length of the unfolded plate were η_x and η_z, respectively, the specified position of the pit can be decided as follows:

$$\begin{aligned} pit_i &\sim pit(x_i, z_i, w_i, d_i); && i = 1, 2, \dots, K \\ x_i &= \eta_x \times random(x_{min}, x_{max}); && i = 1,2, \dots, N \\ z_i &= \eta_z \times random(z_{min}, z_{max}); && i = 1,2, \dots, M+1 \end{aligned} \quad (7)$$

where, x_{min} and x_{max} denote the start and end columns, respectively, in the width of locally pitted area, while z_{min} and z_{max} represent the start and end rows in the length. The diameter w_i and depth d_i of i^{th} pit can be determined through stochastic simulation in terms of the measured data that were obtained from corrosion inspection of in-service structures [28, 30]. Figure 15 shows two simulated tubular members with widespread pitting and localized pitting where the depths of all corrosion pits followed a normal distribution. More details for modelling random pitting corrosion can be found in [28, 30].

3.2. Validation of numerical models

Numerical models of the test specimens were constructed, based on the actual measured sizes of members and corrosion pits shown in Table 1. Material properties from the tensile coupons in Figure 4(b) were used in finite element models. Each model utilized a four-node shell element, Shell 181 that is suitable for analyzing moderately-thick shell structures. The default number of integration points for the single layer model is three; however, the number of integration points is changed to a minimum of five during solution due to the fact that plasticity is present. A fine mesh scheme using 16 elements around each pit was employed, as shown in Figure 15(c), as it has been proven proper to simulate random pitting damage [29, 30]. Fixed-end constraint was applied to a control node at each end of the specimen. The control node was located at the centroid of end cross section and coupled with all the nodes on the end section. At the loading end, however, axial degree of freedom of the control node was released to apply axial displacement to mimic axial compression. Geometrical and material nonlinearities were all taken into account in the numerical analyses. The obtained results were validated against the test results reported above, including load deformation behavior, failure modes and ultimate loads.

Figure 16 shows the load-shortening from numerical analyses. The simulation results of test specimens were collected in two figures to make it more clearly, namely, one for the duplicated specimens and another for the remaining specimens. It was found that good agreements with test results shown in Figure 7 and Figure 8 were obtained. The numerical models built by the proposed modelling method were capable to accurately reproduce all compressive column tests, as shown in

Figure 9. Besides, compressive behavior of pitted test specimens was fully reflected, as shown in Figure 17. In most cases, the relative errors of ultimate loads between numerical and experimental results were no more than 5%, as shown in Table 3 and Figure 18. Slightly larger errors about 7% in Specimens 0-0-3 and 1/4-120-1 resulted from the inevitable eccentric loading induced by the initial deflection.

Since DOV is widely thought suitable to represent the degree of corrosion damage in plated structures [30, 34] and tubular structures [26, 29] that were subject to pitting corrosion damage, Figure 19 shows the relationship of reduction of ultimate strength with the DOVs of all the test specimens. Herein the strength reduction is measured by the ratio of ultimate load of a pitted specimen compared with the control specimen. Two fitting curves were derived respectively for the numerical and experimental results, showing a nonlinear relation between the strength reduction and DOV. A high coincidence between the two fitting curves was attained, further confirming the applicability of the modelling method. Since numerical models were constructed depending on the actually measured sizes, the influence from manufacturing error was also delivered to these models, causing significant variation of numerical results as observed in experimental results, especially for the specimens with non-perforated pits. Also, it could partially be due to the fact that the fitting curves did not involve the shape effect of the corrosion patch but only the DOV. This raises a new demand to conduct further numerical studies upon a unified modelling basis so as to obtain more consistent results.

3.3. Further numerical studies

A new set of numerical models reconstructed in terms of the mean values of measured sizes listed in Table 1 were used to conduct further numerical studies. The mean values of D and t of test specimens were 59.82 and 4.34 mm, respectively, and the mean pit depth was 2.12 mm approximate to 50% wall thickness. For all test specimens, except Specimen 1/4-120-T, new numerical models were established on a unified modelling basis in the sizes of members and corrosion pits, and initial deflection. All simulated specimens were inflicted with the same level of pitting damage with DOP 15% and DOV 8%, except that Specimen 1/4-120-T was subject to DOV 16% due to the perforated pits.

Figure 20 shows the load-shortenings of all simulated specimens. In contrast to results shown in Figure 7 and Figure 8 (experiments) and in Figure 16 (analyses with measured sizes), the effects of corrosion features were exhibited more clearly by the new numerical models. Figure 21 displays consistent trends in the effects of the depth, size, location and shape of corrosion patches, without obvious variation in the simulation results. This makes it more accurate to evaluate the influences of corrosion features on reduction of ultimate strength.

Figure 21(a) shows that the relation of reduction of ultimate load and pit depth was close to linear. The larger pit depth, the larger reduction of ultimate load. Compared with the intact specimen (0-0) with an ultimate load of 327 kN, Specimen 1/4-120 of 50% thickness loss had a reduction of ultimate strength about 6%. However, in Specimen 1/4-120-T, the strength reduction increased up to about 13% nearly double that of Specimen 1/4-120, due to a larger volume loss of material caused by through-thickness pits.

Figure 21(b) indicates that the size change of a corrosion patch had a slight influence on the reduction of ultimate load under the same DOP and DOV. The corrosion patch (S_r = 0.75) caused a reduction of ultimate strength about 6% in Specimen 1/4-120. Compared with this specimen, the increase of patch width in Specimen 1/4-360-M (S_r = 0.25), with the decrease of patch shape ratio, caused a slightly larger decrease in the ultimate load; however, the increase of patch length in Specimen 3/4-120 (S_r = 2.25), with the increase of patch shape ratio, did not cause a decrease but a slight increase in the ultimate load. A far as the same level of localized pitting damage is concerned, the size effect of the corrosion patch seems to be reflected by the shape ratio. It is noteworthy that some disparities existed in the size effect on ultimate loads between tests and numerical analyses. This is ascribed to that the size effect being less obvious under a small DOP was not reflected in the tests; in such case, the random nature of pitting damage and manufacturing error played a dominant role to influence the test results.

Figure 21(c) displays that the location change of the corrosion patch affected the reduction of ultimate strength obviously, under the same pitting damage. Compared with Specimen 1/4-360-E, the corrosion patch in Specimen 1/4-360-M was shifted from one end to mid-height, this resulted in a larger strength reduction. The trend has also been reported in experiments of pitted plates of hull structures [22]. With respect to the location effect, the worst case came from Specimen 1/4-360-B.

As shown in Figure 3, the single patch was split into a dual-patch pattern where two split patches were located at both ends simultaneously with a total area equal to that of the single patch. The dual-patch pattern resulted in a reduction of ultimate strength being more than 7%. This is because the corrosion pits at both ends impaired cross-sections near to endplates which leaded to a serious deterioration of support stiffness from the endplates and then made fixed ends turn into hinged ones.

Figure 21(d) confirms that the reduction of ultimate strength was highly associated with shape ratio of the corrosion patch. In Shape group shown in Table 2, the test specimens had diverse shapes of corrosion patches but with the same corroded area. Understandably, to ensure the same corroded area, the increase of patch width necessarily causes a decrease in patch length, leading to a smaller shape ratio of the corrosion patch; oppositely, the increase of patch length yields a larger shape ratio. Compared with the control specimen, Specimen 1-90 (Sr = 4) had a strength reduction about 3.68%, while the strength reduction in Specimen 1/4-360-M (Sr = 0.25) increased to be about 6.22%. The decrease in the shape ratio made the patch shape transformed from a long-and-narrow pattern to a short-and-wide one. It is apparent that this change resulted in not only an alternation in failure mode, as shown in Figure 9, but an significant effect on ultimate strength. Furthermore, there seems to be a nonlinear relation between the degradation ratio of ultimate strength and the shape ratio, as shown in Figure 22. Therefore, the shape effect of the corrosion patch has a critical effect on the ultimate strength, which should be taken into account for ultimate strength assessment together with the volume loss of corroded material.

4. Discussion

4.1 Mechanism of shape effect

In the column tests, with regard to ultimate loads, three intact specimens (0-0 serials) had the mean strength of 318 kN and standard deviation of 6.1 kN, while the pitted ones (1/4-120 serials) had the mean value of 299 kN and standard deviation of 10.9 kN, respectively. Obviously, variation of the test results in the pitted specimens was more significant than that in the intact ones. This can be attributed to the random natures related to the distribution, size and depth of corrosion pits [29]. In addition, combination of shape effect with initial deflection may affect the variation of the test results due to their influence on failure mode of pitted members, as shown in Figure 9 and Figure 12.

Experimental and numerical studies consistently showed that the corrosion patch of a smaller shape ratio resulted in a larger reduction of ultimate strength than that of a larger shape ratio for the same corroded area. This is because the larger patch width of the smaller shape ratio made random corrosion pits more easily cluster on a certain cross-section. The confluence of pits formed a pit colony leading to a relatively seriously-pitted section than other sections. The pit colony was a hotbed to intensify stress interaction between those pits, initiating the failure on the section. In contrast, a larger patch length of a larger shape ratio made corrosion pits scattered sparsely along the length, lowing the chance to form the pit colony on the section and also alleviating the stress interaction between corrosion pits. For this reason, the failure mode and ultimate strength were drastically affected by the shape of the corrosion patch, as shown in Figure 9. It is apparent that the effects of corrosion features on the compressive behavior of locally pitted members will be more pronounced if higher levels of pitting damages in the Pitting Intensity Diagrams [32] are involved.

4.2 Prediction of ultimate strength

It is common to use volume loss on the weakest section or whole corroded area to quantitate the corrosion effect on the ultimate strength of damaged structures in the existing studies. However, it seems not rational only concerning these factors in view of the results obtained from experiments and numerical analyses herein. Variation of corrosion features of localized pitting, especially shape effect of the corrosion patch, needs to be considered to achieve an accurate strength assessment.

Earlier compressive column tests were conducted upon locally corroded short tubular columns by Ostapenko et al. [35]. Test specimens were subject to patch corrosion where a uniform thickness loss was introduced by grinding to simulate localized uniform corrosion. Based on the results of corroded short columns of $a_n \geq 0.65$, an empirical formula was developed to evaluate ultimate load [35] as:

$$p = \frac{P_u}{P_{yld}} = 0.18a_n + 0.82a_n^3 \qquad (8)$$

where a_n was the relative net area, $a_n = A_n/A_g$, dividing A_n being net area of the corroded section by A_g being gross area of the virgin section. P_u and P_{yld} were respectively ultimate load of the corroded section and original yield load of the intact specimen. As for the test specimens in this paper, the parameter to describe localized uniform corrosion, a_n, is the net area of the weakest cross-section

with the largest number of aligned pits shown in Figure 3, which is listed in Table 3 for each test specimen.

Recent experiments have been carried out upon stub columns with various localized pitting where corrosion pits were randomly drilled on an inclined corroded area of full or half hoop [26]. It was reported that residual strength of a tested short column was proportional to sectional damage ratio. A formula was derived, based on regression analysis on the test results, to predict compressive strength of corroded stub columns [26], given as:

$$RS_c = 1.26R_V - 30.69 \quad (9)$$

where R_V was the ratio of net damaged volume to total volume in the corroded area, and RS_c was the percentage of residual compressive strength compared with the original strength. As for the test specimens studied herein, the R_V can be attained by R_V = 100-DOV in terms of the DOV decided by Eq. (4), and then the RS_c can be determined by Eq. (9).

Figure 23 shows the comparison of results from empirical formulas and numerical analyses with the test results reported in this paper. Obviously, Eqs. (8) and (9) yield conservative estimations on ultimate loads for both intact and pitted specimens. It is noted that the ultimate load predicted by Eq.(8) was highly depended on the yield load in the case of localized uniform corrosion rather than localized pitting [35]. However, the tests conducted in this paper showed that ultimate loads of the test specimens of medium length were at least 20% higher than their yield loads, as shown in Figure 12. On the other side, in order to apply Eq. (8) for calculating the ultimate load, localized pitting was treated as localized uniform corrosion where the maximum pit depth on the weakest cross-section was used to calculate the parameter, a_n, having corrosion damage overestimated. Therefore, it is not rational that locally pitted tubular members are assessed as stub columns with the localized uniform corrosion, depending on the weakest cross sections.

In the experiments [26] used to derive Eq.(9), localized pitting was induced in a pattern on half or full of the circumference, which was, in some extent, similar to considering the size effect of the corrosion patch. The reduction of ultimate strength seemed to result from the volume loss rather than the size effect, being similar to that observed in the tests of this paper. However, the prediction on the ultimate load in terms of Eq. (9) was often overly conservative. For all test specimens, the lowest estimate occurred in Specimen 1-90, being about 13.7% lower than the test result. Actually,

failure behavior of pitted members was not necessarily affected by localized pitting, particularly for the corrosion patch in a long-and-narrow shape, as shown in Figure 9 (c). However, such shape effect was not taken into account in this formula. Even for the intact members, Specimens 0-0 series with DOV 0% and R_V = 100, the strength yielded by Eq. (9), RS_c, is 95.31 being 4.69% below the actual strength. Therefore, locally pitted members of medium length that collapses by interactive buckling or column buckling cannot also be assessed as stub columns.

By contrast, the proposed modelling method in this paper can be used to accurately predict the ultimate strength of locally pitted tubular members in terms of actually measured sizes despite the shortage of detailed suggestions on how to model actual corrosion in the current Specifications [10, 11]. Effects of corrosion features including the depth, size, location and shape of the corrosion patch have been clearly clarified based on the experimental and numerical studies in this paper. Nevertheless, there are some difficulties to develop an empirical formula for compressive strength of locally pitted tubular members only based on the limited column tests. However, it is possible to derive the empirical formula through performing numerous stochastic simulations on the basis of the proposed modelling method.

5. Conclusion

Compressive column tests in conjunction with corresponding numerical studies have been carried out on tubular members with/without localized pitting corrosion to study compressive behavior and ultimate strength. Numerical models to describe pit details were built using a novel modelling method, and validated against the experiments. Highly consistent results between the experiments and numerical analyses were achieved in the load deformation behavior, load strain behavior and failure mode. Effects of the depth, size, location and shape of the corrosion patch on the reduction of ultimate strength were experimentally and numerically explored and clarified.

The tests of locally pitted tubular members herein provide a benchmark to calibrate numerical modelling. Numerical modelling on the basis of actually measured sizes can replicate all the column tests, yielding consistent predictions. Moreover, the strength reduction of locally pitted members is highly and positively correlated with pit depth. The shape change of the locally corroded area has a critical impact to compressive behavior and ultimate strength, due to stress interaction resulting from the pit cluster, likely change the failure mode. The shape ratio of the locally pitted area is a

key factor that needs to be considered together with volume loss of corroded material for ultimate strength assessment.

Acknowledgement

The first author would like to thank the National Natural Science Foundation of China [grant number 51879124] for the financial support, and appreciate Mr. Chaoming Shen from the Engineering Mechanics Laboratory at the Jiangsu University of Science and Technology for his assistance during the experimental study.

References

[1] Wang Y, Wharton JA, Shenoi RA. Ultimate strength analysis of aged steel-plated structures exposed to marine corrosion damage: A review. Corrosion Science. 2014;86:42-60.

[2] ABS. Buckling and ultimate strength assessment for offshore structures. Houston: American Bureau of Shipping; 2014.

[3] Pidaparti RM, Rao AS. Analysis of pits induced stresses due to metal corrosion. Corrosion Science. 2008;50:1932-8.

[4] Cerit M. Corrosion pit-induced stress concentration in spherical pressure vessel. Thin-Walled Structures. 2019;136:106-12.

[5] Dewanbabee H, Das S. Structural behavior of corroded steel pipes subject to axial compression and internal pressure: Experimental study. Journal of Structural Engineering. 2013;139:57-65.

[6] Rajabipour A, Melchers RE. A numerical study of damage caused by combined pitting corrosion and axial stress in steel pipes. Corrosion Science. 2013;76:292-301.

[7] Ahmadi H, Mayeli V. Development of a probability distribution model for the LJF factors in offshore two-planar tubular DK-joints subjected to OPB moment loading. Marine Structures. 2019;63:196-214.

[8] Ahmadi H, Mayeli V. Probabilistic analysis of the local joint flexibility in two-planar tubular DK-joints of offshore jacket structures under in-plane bending loads. Applied Ocean Research. 2018;81:126-40.

[9] Vaz MA, Cyrino JCR, Hernández ID, Zegarra VD, Martinez JL, Liang DA. Experimental and numerical analyses of the ultimate compressive strength of perforated offshore tubular members. Marine Structures. 2018;58:1-17.

[10] ISO19902. Petroleum and natural gas industries – Fixed steel offshore structures. Geneva: the International Organization for Standardization; 2007.

[11] ASME-B31G. Manual for determining the remaining strength of corroded pipelines. Washington: American Society of Mechanical Engineers; 2012.

[12] Hebor ME, Rieles JM. Local buckling strength of patch corrosion damaged steel tubular bracing. International Journal of Steel Structures. 2002;2:59-70.

[13] Karagah H, Shi C, Dawood M, Belarbi A. Experimental investigation of short steel columns with localized corrosion. Thin-Walled Structures. 2015;87:191-9.

[14] Shi C, Karagah H, Dawood M, Belarbi A. Numerical investigation of H-shaped short steel piles with localized severe corrosion. Engineering Structures. 2014;73:114-24.

[15] Sadovský Z, Drdácký M. Buckling of plate strip subjected to localised corrosion—a stochastic model. Thin-Walled Structures. 2001;39:247-59.

[16] Dunbar TE, Pegg N, Taheri F, Jiang L. A computational investigation of the effects of localized corrosion on plates and stiffened panels. Marine Structures. 2004;17:385-402.

[17] Chen Y, Li X, Chai YH, Zhou J. Assessment of the flexural capacity of corroded steel pipes. International Journal of Pressure Vessels and Piping. 2010;87:100-10.
[18] Motta RS, Cabral HLD, Afonso SMB, Willmersdorf RB, Bouchonneau N, Lyra PRM, et al. Comparative studies for failure pressure prediction of corroded pipelines. Engineering Failure Analysis. 2017;81:178-92.
[19] Shariati M, Rokhi MM. Numerical and experimental investigations on buckling of steel cylindrical shells with elliptical cutout subject to axial compression. Thin-Walled Structures. 2008;46:1251-61.
[20] Yao Y, Yang Y, He Z, Wang Y. Experimental study on generalized constitutive model of hull structural plate with multi-parameter pitting corrosion. Ocean Engineering. 2018;170:407-15.
[21] Sheng J, Xia J. Effect of simulated pitting corrosion on the tensile properties of steel. Construction and Building Materials. 2017;131:90-100.
[22] Nakai T, Matsushita H, Yamamoto N, Arai H. Effect of pitting corrosion on local strength of hold frames of bulk carriers (1st report). Marine Structures. 2004;17:403-32.
[23] Nakai T, Matsushita H, Yamamoto N. Effect of pitting corrosion on local strength of hold frames of bulk carriers (2nd Report) – Lateral-distortional buckling and local face buckling. Marine Structures. 2004;17:612-41.
[24] Shi XH, Zhang J, Guedes Soares C. Numerical assessment of experiments on the ultimate strength of stiffened panels with pitting corrosion under compression. Thin-Walled Structures. 2018;133:52-70.
[25] Zhang J, Shi XH, Guedes Soares C. Experimental analysis of residual ultimate strength of stiffened panels with pitting corrosion under compression. Engineering Structures. 2017;152:70-86.
[26] Ahn J-H, Choi WR, Jeon SH, Kim S-H, Kim I-T. Residual compressive strength of inclined steel tubular members with local corrosion. Applied Ocean Research. 2016;59:498-509.
[27] Sun J, Cheng YF. Assessment by finite element modeling of the interaction of multiple corrosion defects and the effect on failure pressure of corroded pipelines. Engineering Structures. 2018;165:278-86.
[28] Wang R, Sun J, Fang Y. The parameterization construction method of numerical model of cylindrical shells with random pitting corrosion. China. China Patent Bureau: 2018, ZL201510238911.2.
[29] Wang R, Shenoi RA. Experimental and numerical study on ultimate strength of steel tubular members with pitting corrosion damage. Marine Structures. 2019;64:124-37.
[30] Wang R, Shenoi RA, Sobey A. Ultimate strength assessment of plated steel structures with random pitting corrosion damage. Journal of Constructional Steel Research. 2018;143:331-42.
[31] EN-1993-1-1. Eurocode 3: Design of steel structures—Part 1-1 : General rules and rules for buildings. Brussels: European Committee for Standardisation; 2004.
[32] IACS. Requirements concerning survey and certification. London: International Association of Classification Societies; 2016.
[33] Garbatov Y, Tekgoz M, Soares CG. Experimental and numerical strength assessment of stiffened plates subjected to severe non-uniform corrosion degradation and compressive load. Ships and Offshore Structures. 2017;12:461-73.
[34] Saad-Eldeen S, Garbatov Y, Guedes Soares C. Buckling collapse tests of deteriorated steel plates with multiple circular openings. Ocean Engineering. 2019;172:523-30.
[35] Ostapenko A, Berger TW, Chambers SL, Hebor MF. Corrosion damage effect on strength of tubular columns with patch corrosion. Bethlehem: Lehigh University; 1996.

List of Figures and Tables

Figures

(a)  (b) 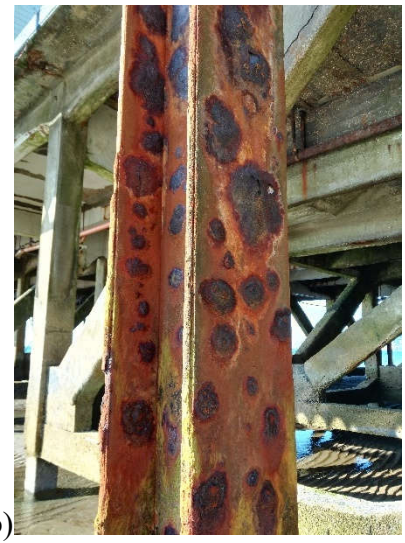

Figure 1 Locally pitted steel members. (a) Tubular column; (b) H section column.

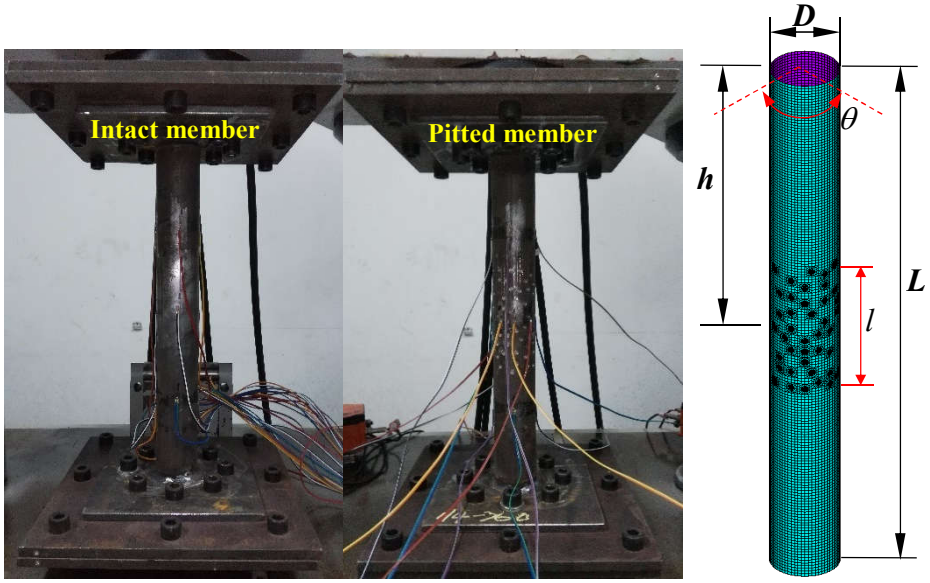

Figure 2 Geometric parameters of test specimens.

No.	1/4-120	3/4-120	1-90
Random pits on partial perimeter	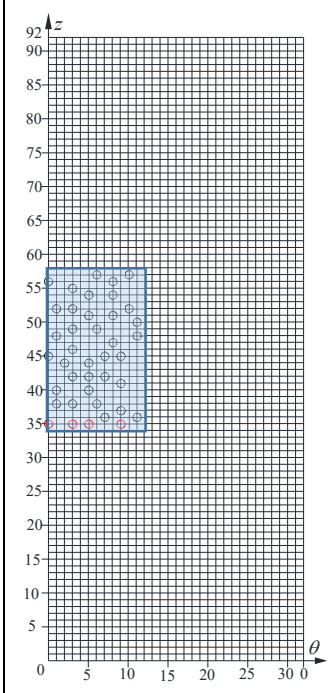	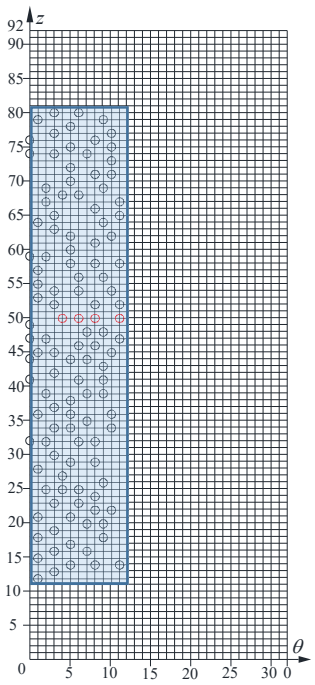	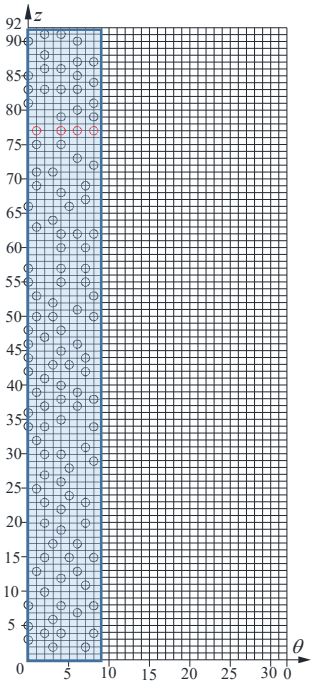
No.	1/4-360-M	1/4-360-B	1/4-360-E
Random pits on full perimeter	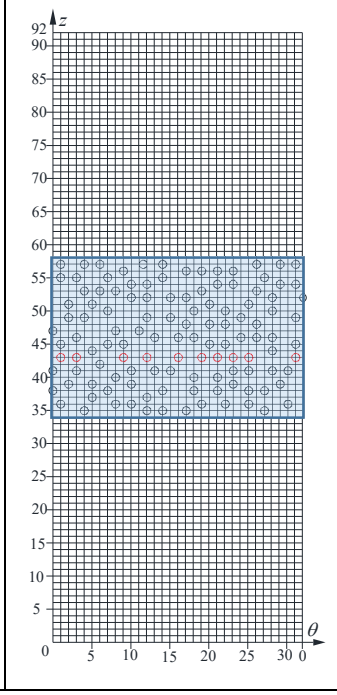	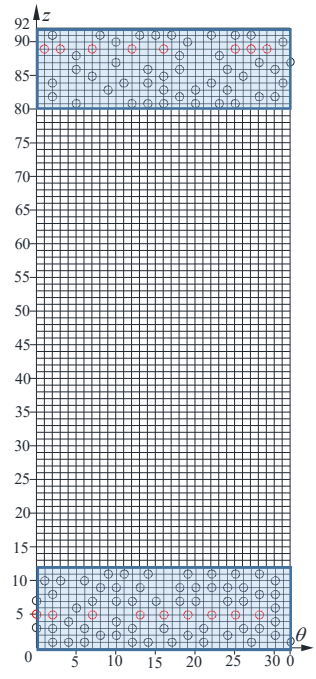	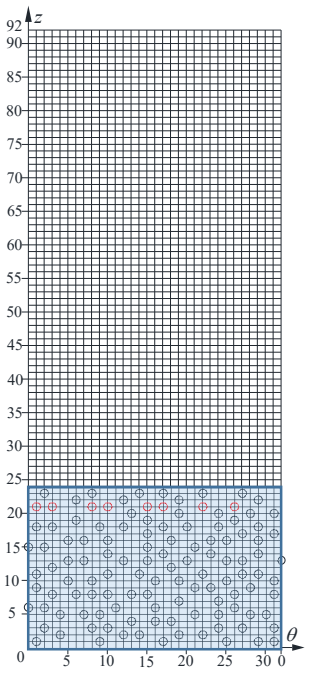

Note: The section with corrosion pits, shown by the red circles, is the weakest cross-section in each pitted specimen.

Figure 3 Pitting patterns on unfolded outside surface of test specimens.

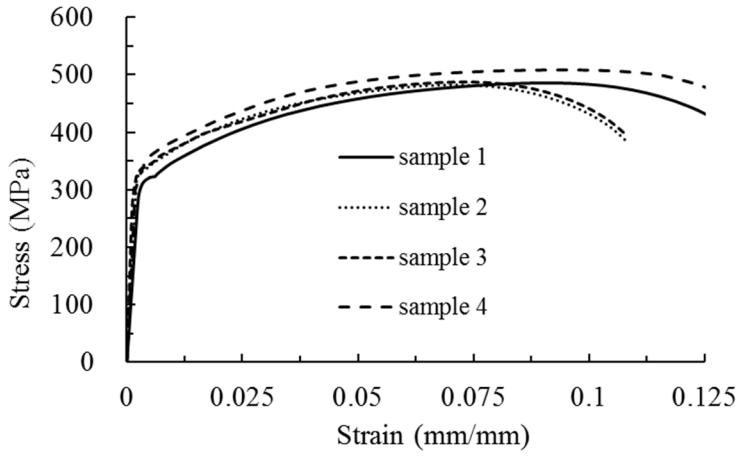

(a)

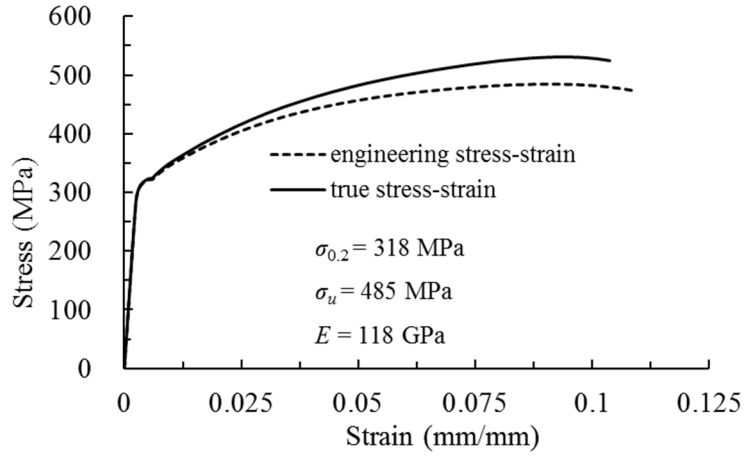

(b)

Figure 4 Material properties of tensile coupons of test specimens. (a) Average stress-strain curves of tensile coupons; (b) stress-strain curve for numerical analysis.

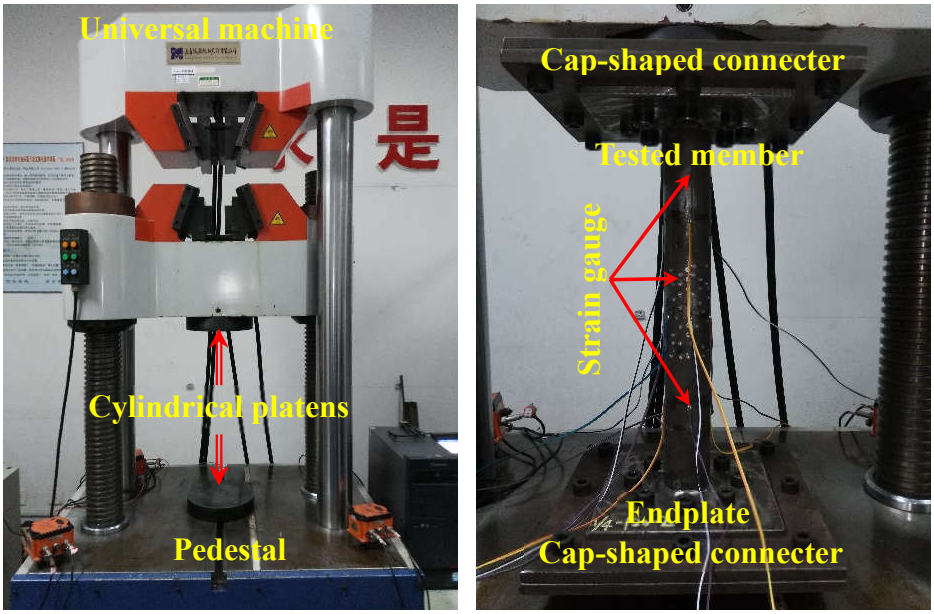

Figure 5 Experimental setup of compressive column tests.

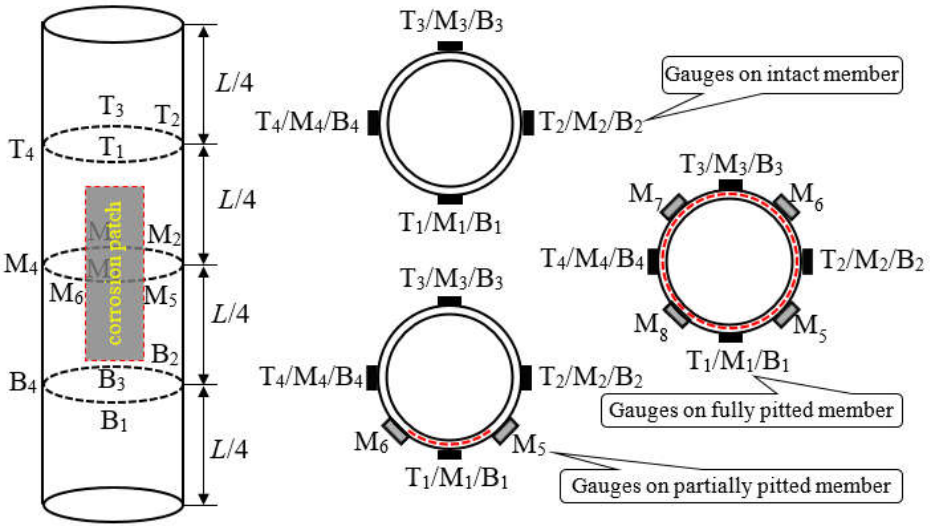

Figure 6 Schematic of strain gauges anchored on test specimens.

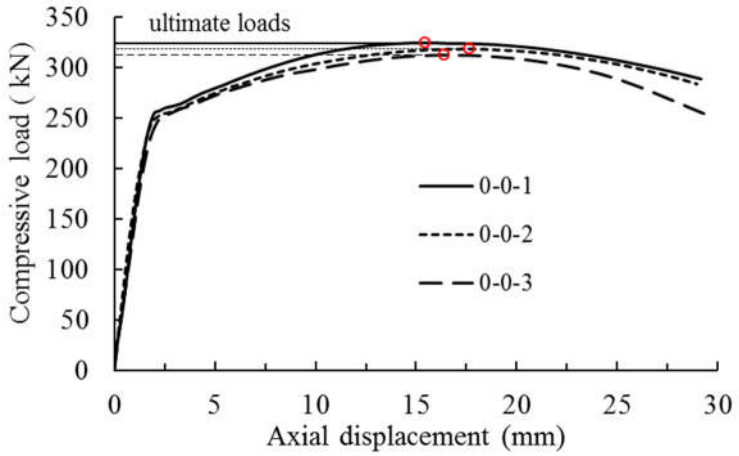

(a)

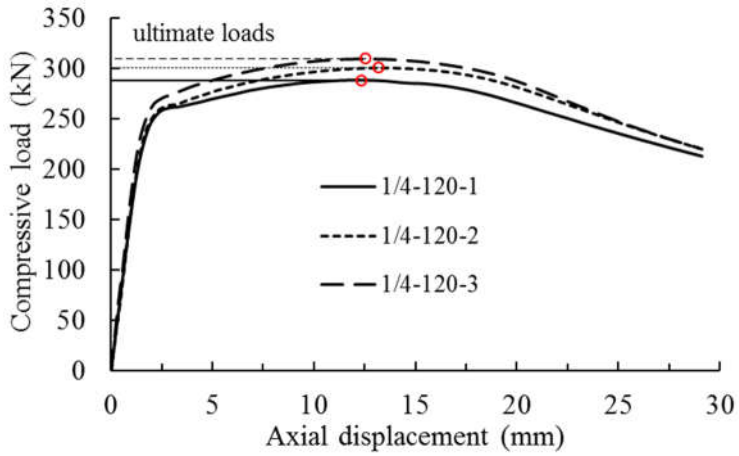

(b)

Figure 7 Load deformation behavior of intact and pitted test specimens. (a) Intact specimens; (b) pitted specimens.

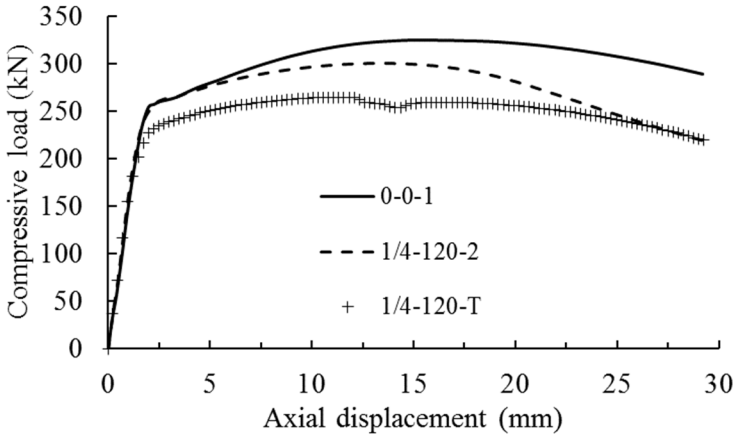
Compressive load (kN)
350
300
250
200
150
100
50
0
0
5
10
15
20
25
30
Axial displacement (mm)
0-0-1
1/4-120-2
1/4-120-T

(a)

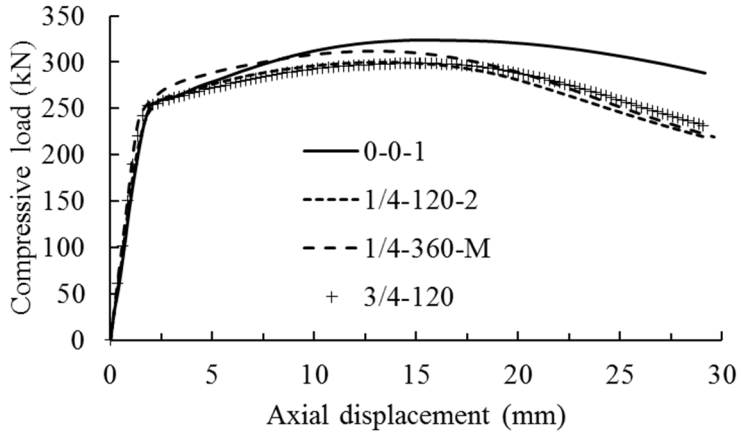
Compressive load (kN)
350
300
250
200
150
100
50
0
0
5
10
15
20
25
30
Axial displacement (mm)
0-0-1
1/4-120-2
1/4-360-M
3/4-120

(b)

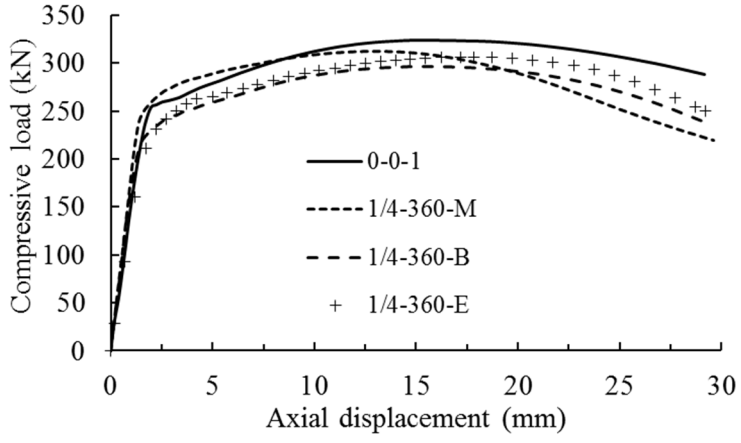
Compressive load (kN)
350
300
250
200
150
100
50
0
0
5
10
15
20
25
30
Axial displacement (mm)
0-0-1
1/4-360-M
1/4-360-B
1/4-360-E

(c)

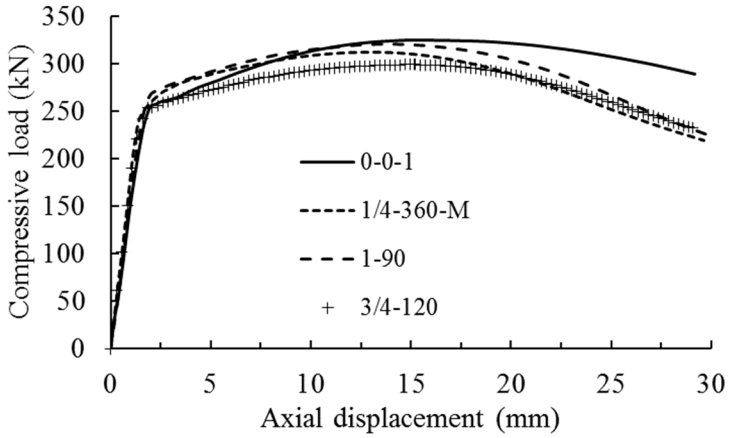

(d)

Figure 8 Experimental load-shortening of test specimens. (a) Depth group; (b) Size group; (c) Location group; (d) Shape group.

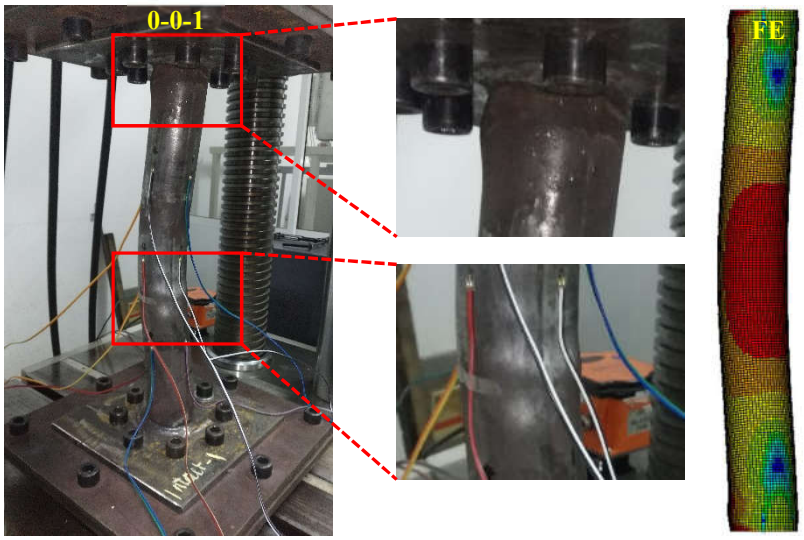

(a)

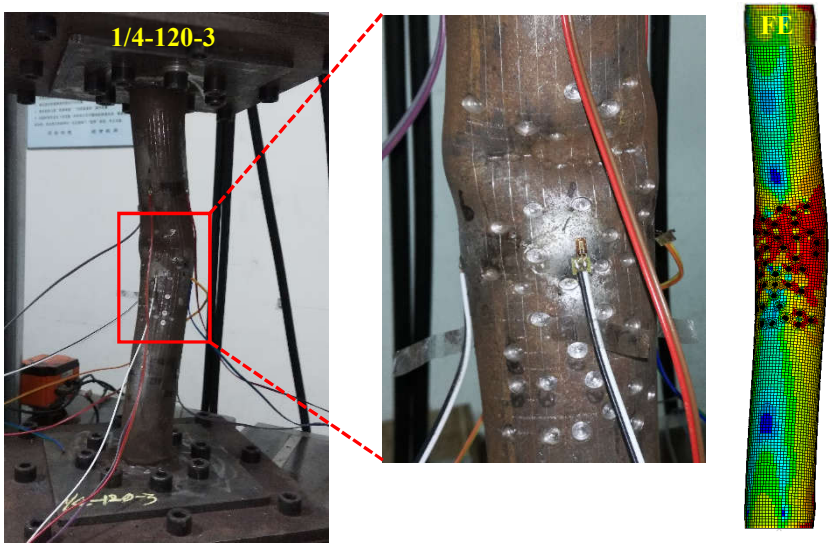

(b)

(c)

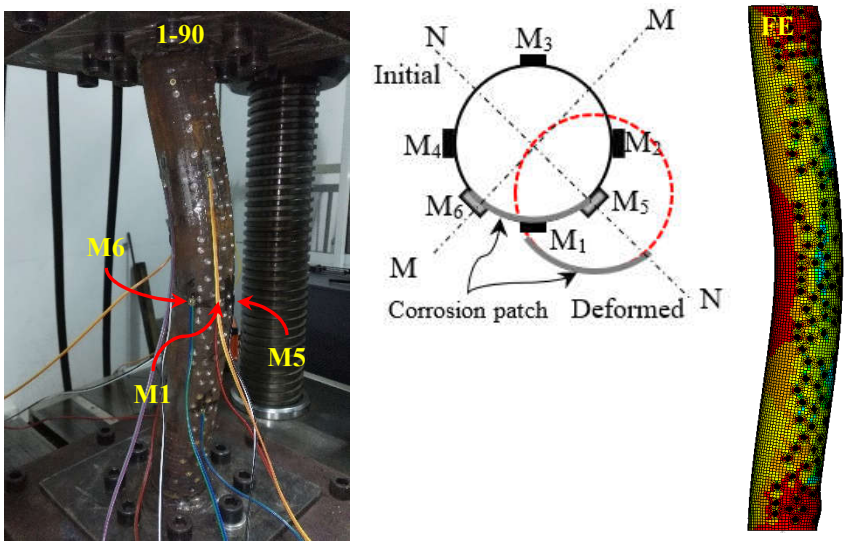

Figure 9 Compressive behavior of intact and pitted specimens. (a) Failure mode of intact specimens dominated by initial deflection; (b) failure mode of pitted specimens due to pitting damage; (c) atypical failure mode of a pitted specimen dominated by initial deflection.

(a)

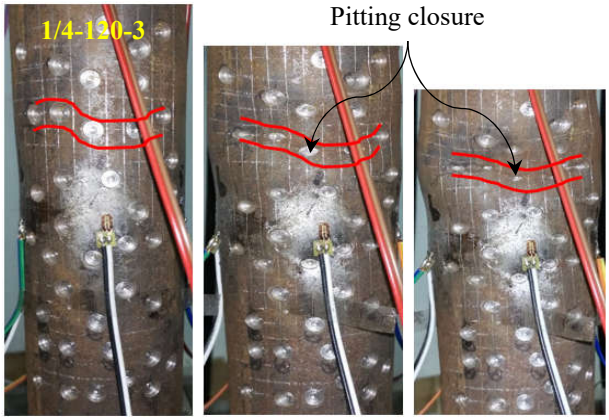

(b)

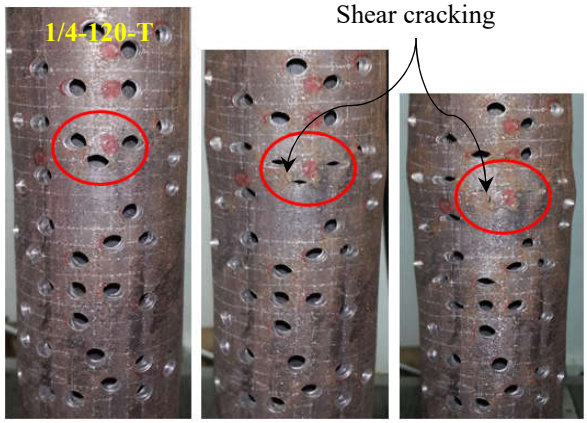

Figure 10 Failure behavior of locally pitted areas. (a) A specimen with non-perforated pits; (b) a specimen with perforated pits.

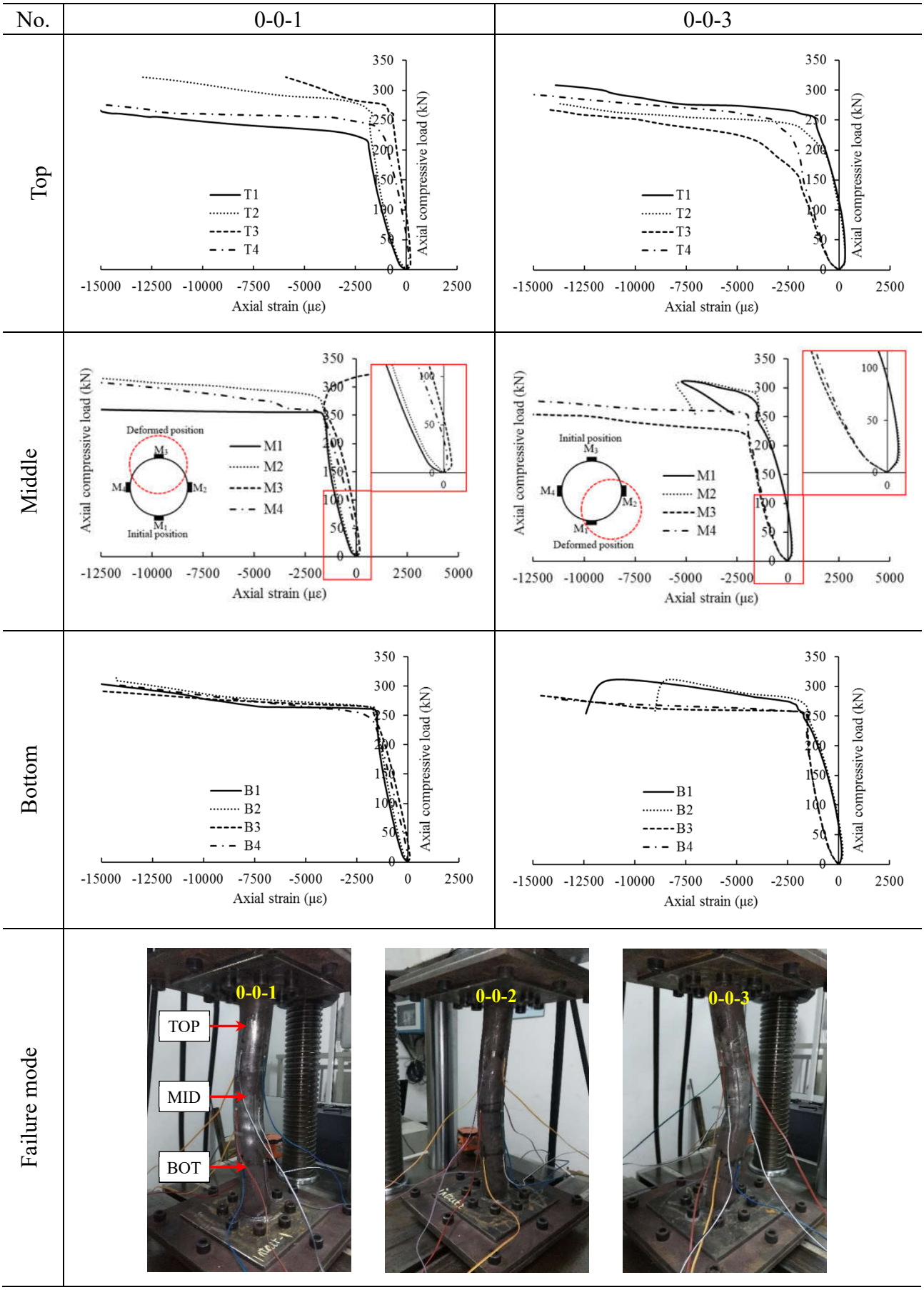

Figure 11 Axial strains along the length of intact test specimens.

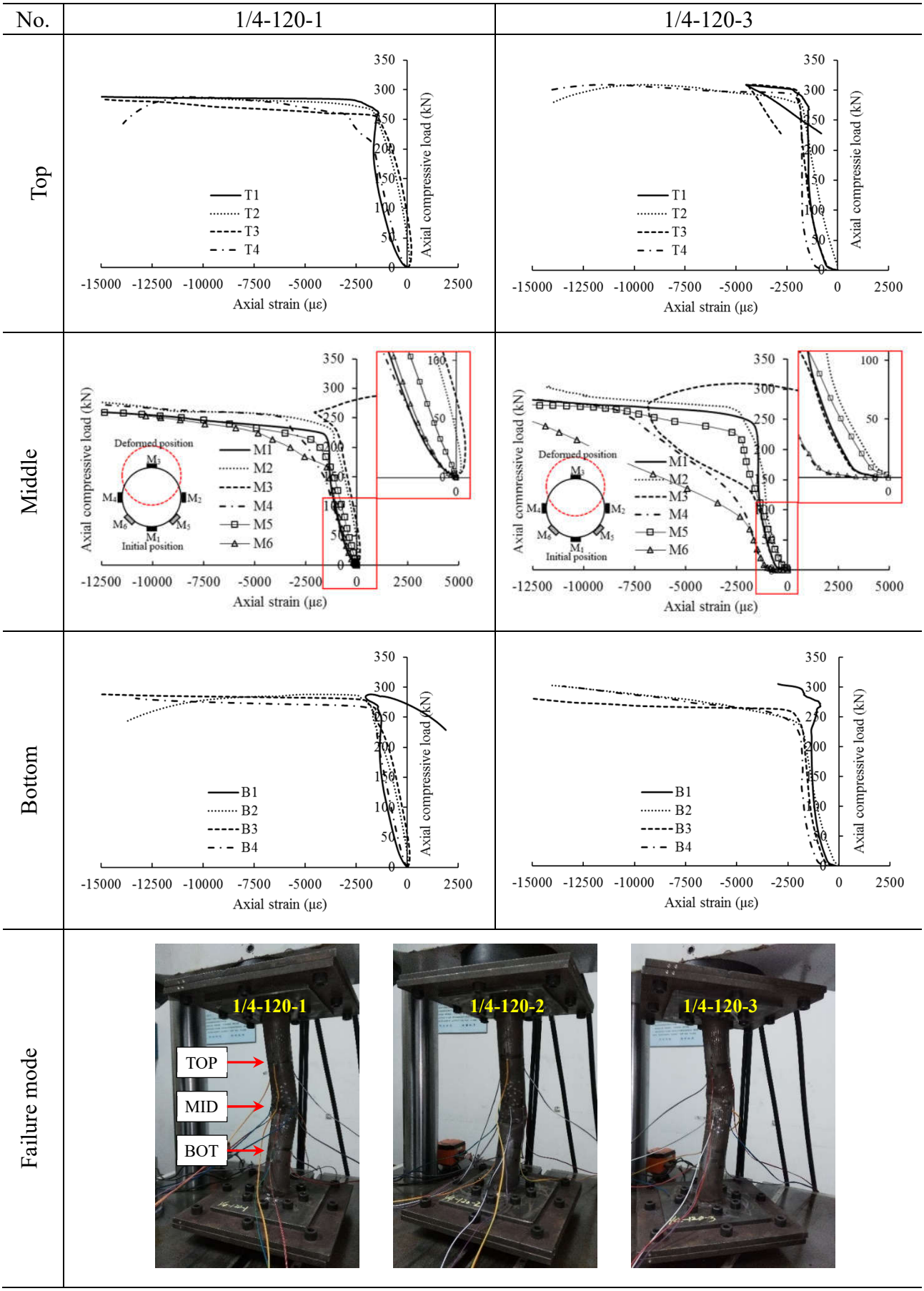

Figure 12 Axial strains along the length of pitted test specimens.

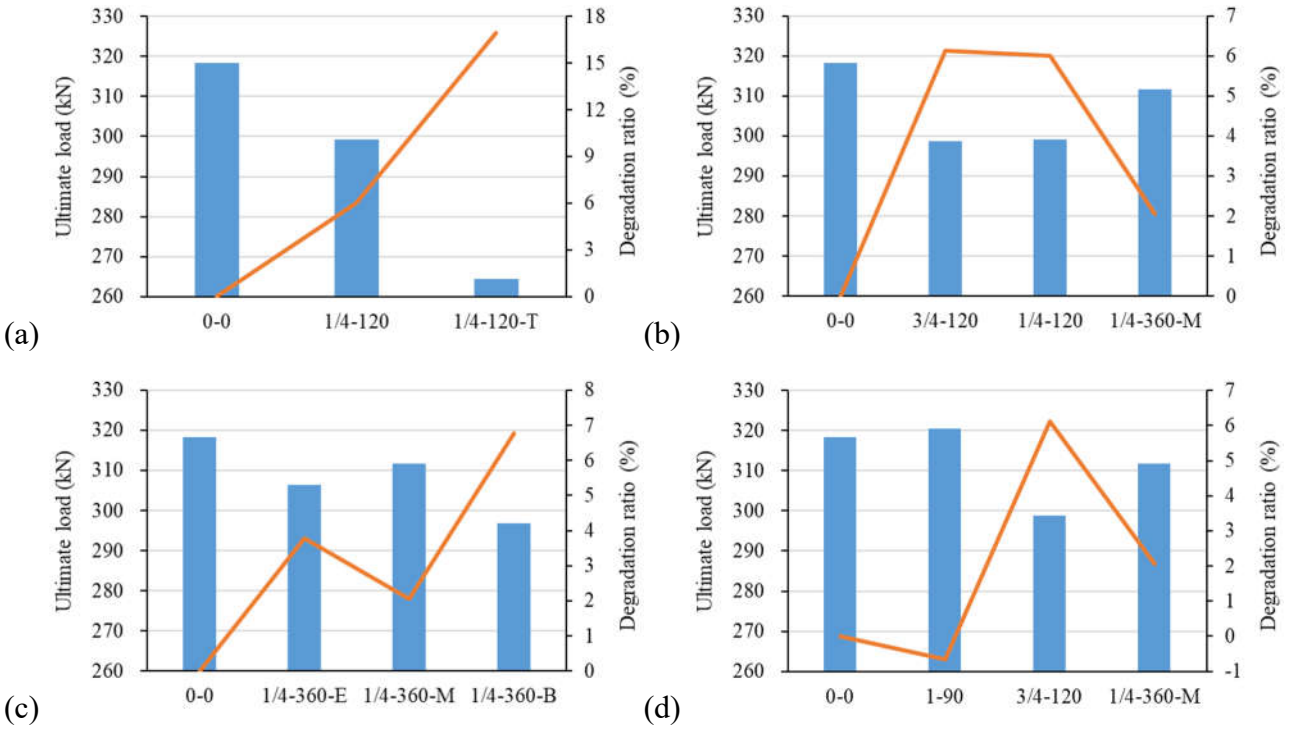

Figure 13 Effects of corrosion features on ultimate loads of pitted specimens. (a) Depth effect; (b) size effect; (c) location effect; (d) shape effect.

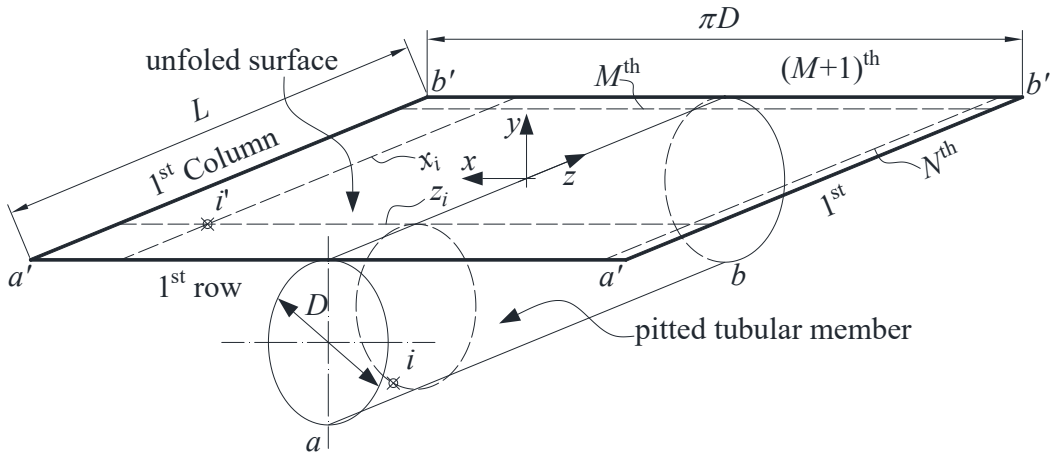

Figure 14 Unfolded outside surface of a pitted member.

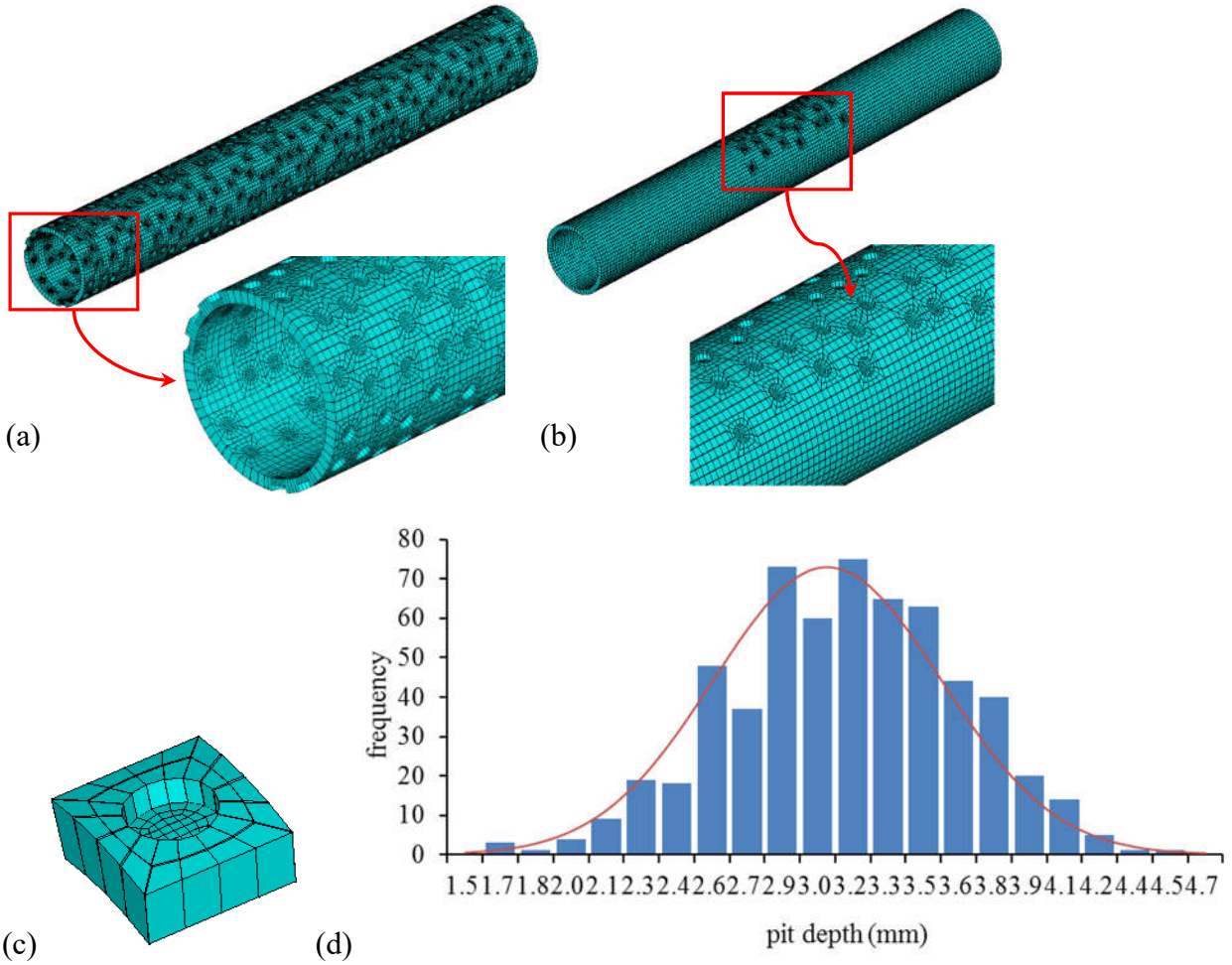

Figure 15 Simulated tubular members with random pitting corrosion. (a) Widely pitted member; (b) locally pitted member; (c) detailed pit model; (d) probabilistic depths of random pits.

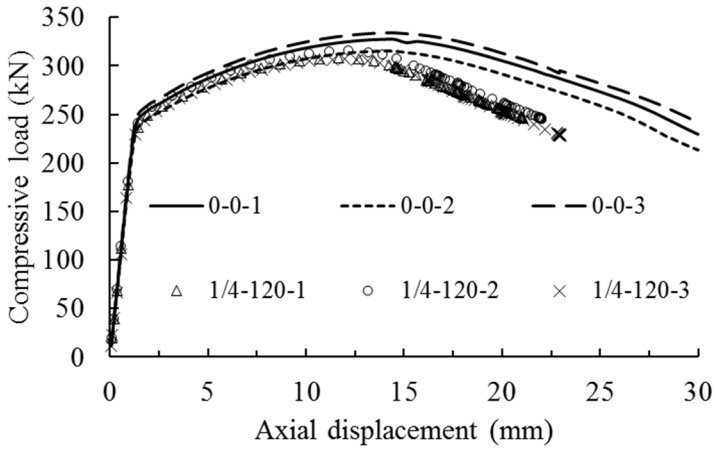

(a)

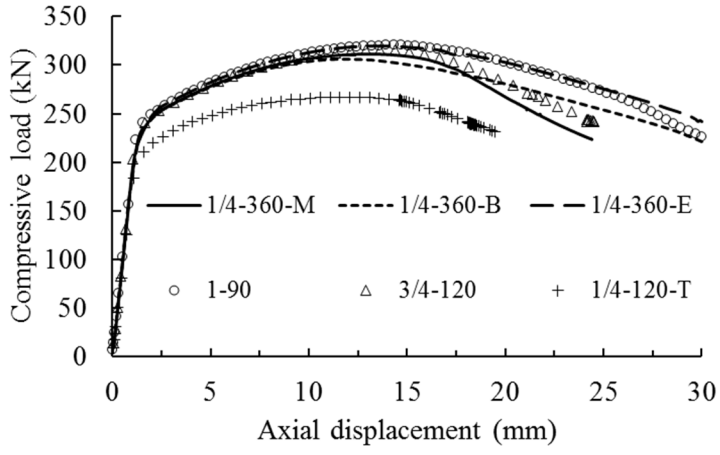

(b)

Figure 16 Load-shortening of test specimens simulated with actually measured sizes. (a) Duplicated specimens; (b) remaining specimens.

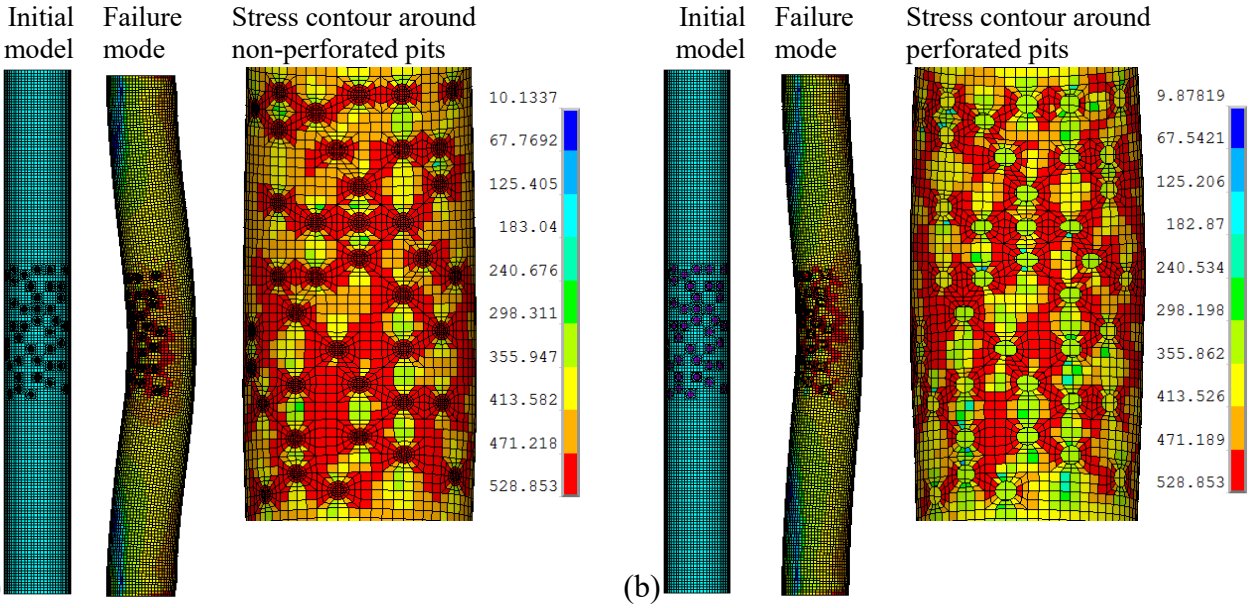

(a) (b)

Figure 17 Von Mises stress (MPa) of typical test specimens simulated with actually measured sizes. (a) 1/4-120-3; (b) 1/4-120-T.

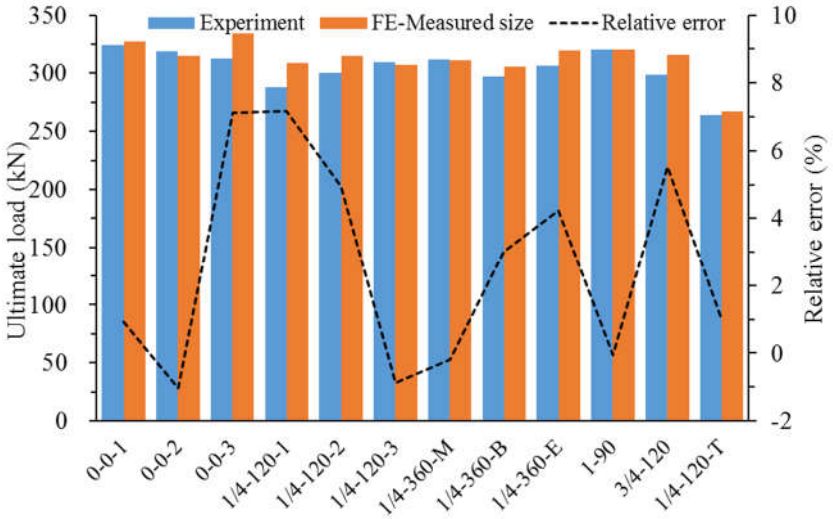

Figure 18 Comparison of ultimate loads between experiments and numerical analyses.

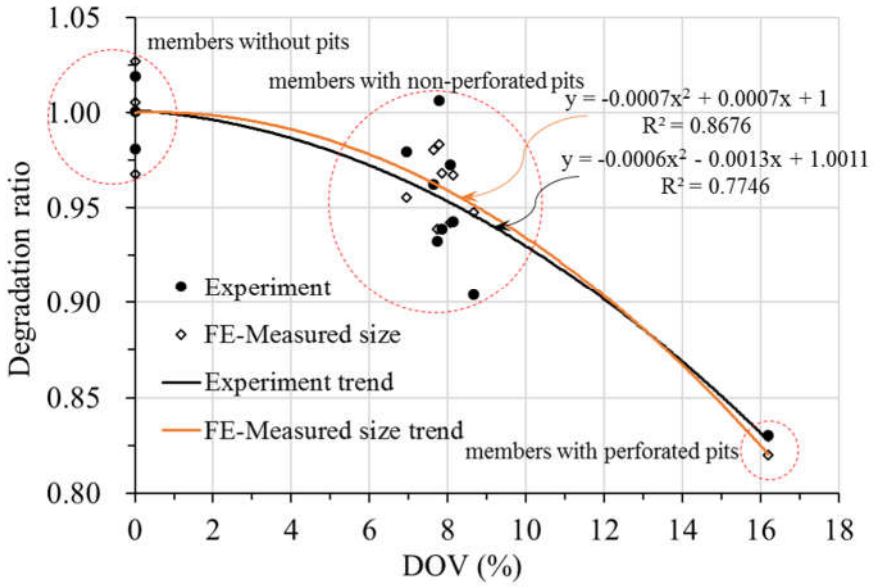

Figure 19 Degradation ratio of ultimate strength of pitted members versus DOV.

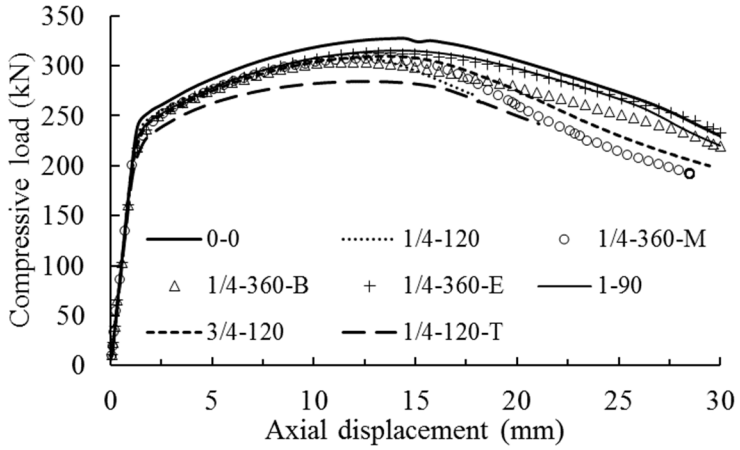

Figure 20 Numerical load-shortening of test specimens with mean values of measured sizes.

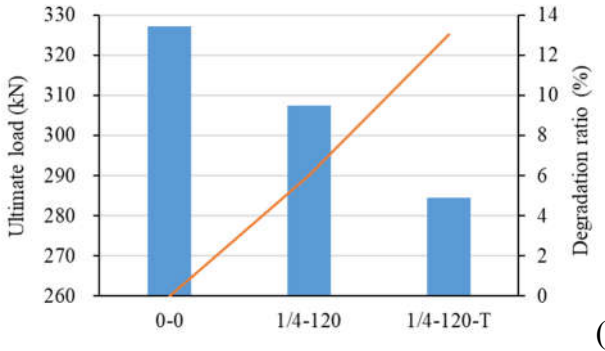

(a)

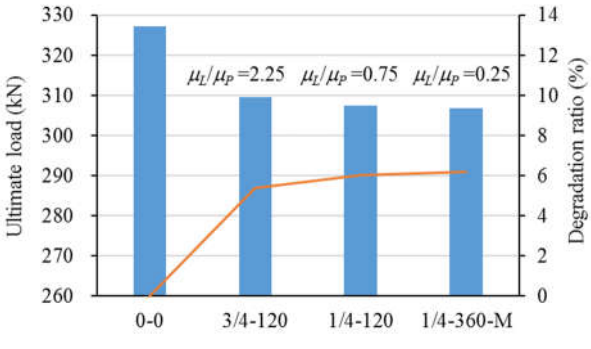

(b)

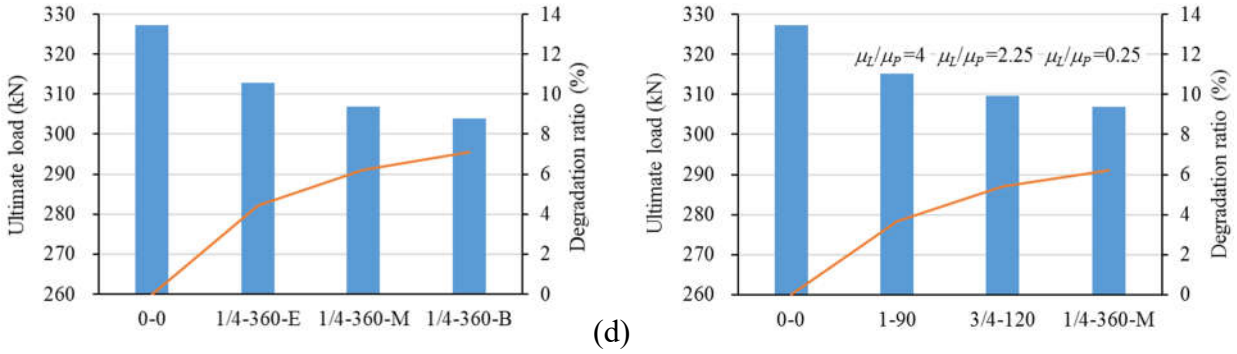

Figure 21 Effects of corrosion features on numerical ultimate loads of pitted members. (a) Depth effect; (b) size effect; (c) location effect; (d) shape effect.

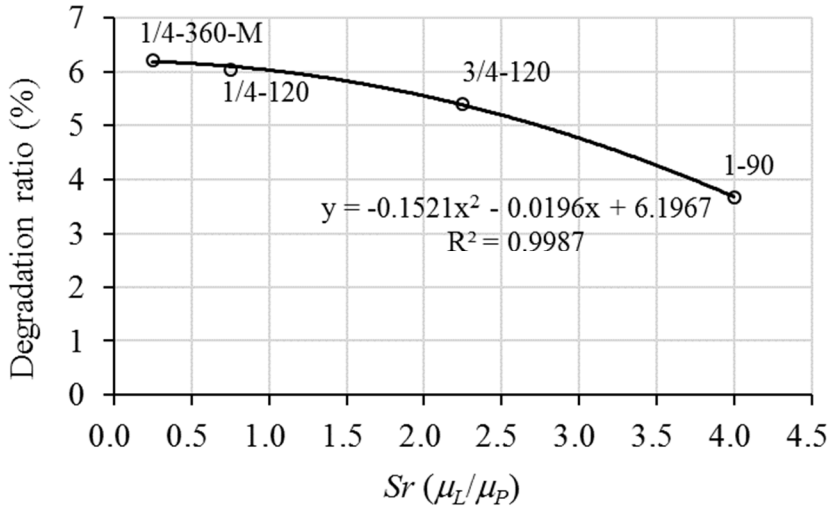

Figure 22 Shape effect on strength reduction of pitted members.

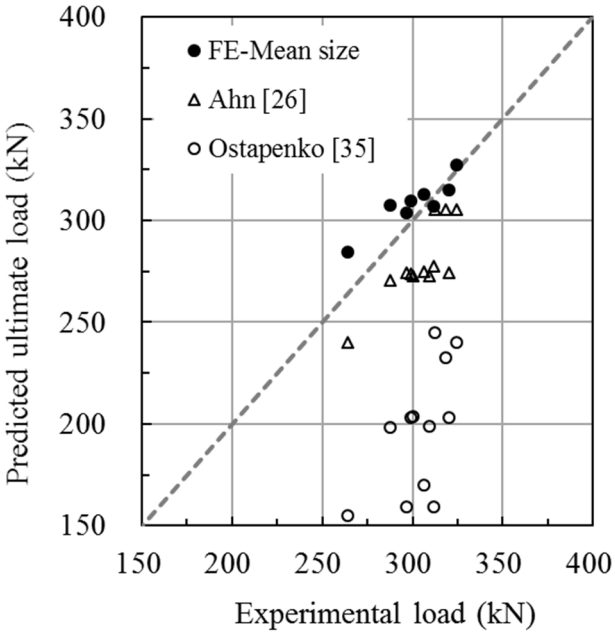

Figure 23 Comparison of ultimate loads from various empiric formulas with test results.

Tables

Table 1 Matrix of test specimens.

Test	No.	L (mm)	D (mm)	t (mm)	μ_L	μ_P	h	K	d (mm)	r (mm)	DOV (%)
1	0-0-1	480	59.83	4.33							
2	0-0-2	480	59.59	4.20							
3	0-0-3	480	59.61	4.44							
4	1/4-120-1	480	59.95	4.36	1/4	1/3	L/2	40	2.33	3	8.65
5	1/4-120-2	480	59.98	4.42	1/4	1/3	L/2	40	2.22	3	8.14
6	1/4-120-3	480	59.97	4.31	1/4	1/3	L/2	40	2.15	3	8.07
7	1/4-360-M	480	59.93	4.33	1/4	1	L/2	120	1.86	3	6.95
8	1/4-360-B	480	59.74	4.35	1/4	1	L/16	120	2.07	3	7.73
9	1/4-360-E	480	59.64	4.42	1/4	1	L/2	120	2.07	3	7.63
10	1-90	480	59.93	4.38	1	1/4	L/2	120	2.10	3	7.77
11	3/4-120	480	59.95	4.39	3/4	1/3	L/2	120	2.13	3	7.86
12	1/4-120-T	480	59.66	4.10	1/4	1/3	L/2	40	4.10	3	16.20

Table 2 Attributes to group test specimens.

Group	Test	Member	Attribute
Control	1, 2, 3	0-0 serials	three intact specimens without pits
Depth	4, 5, 6	1/4-120 serials	three duplicated pitted specimens
	12	1-/4-120-T	one specimen with perforated pits
Size	4, 5, 6	1/4-120 serials	three duplicated pitted specimens
	7	1/4-360-M	one specimen with full hoop corrosion
	11	3/4-120	one specimen with a larger pitted length
Location	7	1/4-360-**M**	the same number of pits at **M**id-height
	8	1/4-360-**B**	the same number of pits at **B**oth ends
	9	1/4-360-**E**	the same number of pits at one **E**nd
Shape	7	1/4-360-M	one corrosion patch of the same corroded area
	10	1-90	but different shape ratios
	11	3/4-120	

Table 3 Experimental and numerical results of ultimate loads of test specimens.

Test	No.	μ_L/μ_P	$\mu_L\mu_P$	n	$a_n=A_n/A_g$	Test (kN)	FE (kN)	(1-FE/Test)×100%
1	0-0-1				1.0	324.4	327.3	0.92
2	0-0-2				1.0	318.4	315.2	-1.02
3	0-0-3				1.0	312.2	334.4	7.12
4	1/4-120-1	3/4	1/12	4	0.927	287.8	308.5	7.18
5	1/4-120-2	3/4	1/12	4	0.931	300.1	315.0	4.94
6	1/4-120-3	3/4	1/12	4	0.932	309.6	306.8	-0.88
7	1/4-360-M	1/4	1/4	10	0.852	311.8	311.2	-0.19
8	1/4-360-B	1/4	1/4	9	0.852	296.8	305.7	3.02
9	1/4-360-E	1/4	1/4	8	0.870	306.3	319.3	4.23
10	1-90	4	1/4	4	0.934	320.4	320.2	-0.04
11	3/4-120	9/4	1/4	4	0.933	298.8	315.3	5.53
12	1-/4-120-T	3/4	1/12	4	0.863	264.3	267.0	1.02